OBJECT-BASED IMAGE ANALYSIS APPLIED FOR DIFFERENT STAGES OF RUBBER PLANTATIONS MAPPING USING THAICHOTE SATELLITE DATA

[1,2]WASANA PUTKLANG, [1]CHARAT MONGKOLSAWAT,

[1,2]RASAMEE SUWANWERAKAMTORN

[1]Department of Computer Science, Faculty of Science, Khon Kaen University, Khon Kaen Thailand

[2]Geo-Informatics Centre for Development of Northeast Thailand, Faculty of Science, Khon Kaen

University, Khon Kaen Thailand

E-mail: [1]putklang_w@kku.ac.th, [2]charat@kku.ac.th, [3]rasamee@kku.ac.th

ABSTRACT

During 2000 to 2011, rubber plantations rapidly expanded in northeast Thailand, which had not been historically planted. Information about planted areas and their distribution is a prerequisite for formulating land use planning and understanding its consequences on ecosystems. This study aimed to establish a model for digitally devising a synergistic approach to distinguishing the different stages of rubber plantations in the northeasternmost region of Thailand and a small portion of the Lao People's Democratic Republic (Lao PDR). The combination of Object-Based Image Analysis (OBIA), Vegetation Canopy Density (VCD), plant phenology and intensive ground observation was applied to THAICHOTE satellite data. Two levels of classification based on OBIA approach were performed. At the first level, multi-scale image segmentation of pansharpened imagery was performed to divide the image set into objects with different spectral and spatial characteristics. Incorporating the normalized difference vegetation index (NDVI) and brightness index (BI) into the objects, the image set was subdivided into four different subsets of VCD. Analyses were then performed at the next level classification on each of VCD subsets by using certain and a range of different approaches to discriminate stand age rubber tree plantations. Rubber tree phenology and OBIA feature optimization were used to differentiate the different stages of rubber plantations. The results indicated that the agreement between field-based classification and image-based classification was well correlated. The overall accuracy of 79.00 % and Cohen's kappa coefficient of 0.77 were achieved for the integrated models for the different stage of rubber plantations.

Keywords: *THAICHOTE satellite data; Different stages of rubber plantations; Object-based image analysis (OBIA); Vegetation canopy density (VCD); Plant phenology; Northeast Thailand*

1.   INTRODUCTION

Natural rubber (Hevea brasiliensis Muell. Arg) is the main economic crop cultivated in southern Thailand, where climatic conditions and land qualities are highly suitable. Rubber trees were not historically planted in northeast Thailand. Over the past fifteen years, with an attractive price for rubber products, northeast farmers switched and diversified their lands to cultivate rubber trees instead of the traditional crops (cassava and sugar-cane) that had been cultivated for many decades. The world production of natural rubber amounted to 7.9 million tons in 2003, of which Thailand contributed approximately 36% [1]. In 2016, the world production of natural rubber reached 12.40 million tons [2]. Thailand's rubber production has been the world's largest by export volume, accounting for 30.31% of the world market [3]. The rapidly increasing expansion provoked competition for the scarce uplands, which led to encroachment on the government's conservative forests and low land paddy fields marginally suitable for the rubber trees [4]. Rubber exporters posted declines from 2012 to 2016, with a surplus of rubber production and unattractive prices. The Thai government has attempted to decrease the surplus of rubber production by logging rubber trees cultivated in forest reserves and the increase in domestic use. Information about rubber plantation areas and their

spatial distribution is a prerequisite for global sales of natural rubber products, strategic planning, agricultural extension, and sustainable land use planning. In addition to these applications, data on rubber plantation areas and their spatial distribution may have significant impacts and consequences on land ecosystems when indigenous, ecological forests are replaced by rubber plantations.

With the advent of satellite technology and the high capability of computers, information about cropping areas and covering types over the ground surface, including resource management and environmental issues has been updated rapidly. Several studies have been conducted by using the traditional pixel-based image analysis (PBIA) of vegetation indices to discriminate rubber-planted areas. One study investigating the potential of Pléiades data and three selected vegetation indices (the normalized difference vegetation index (NDVI) enhanced vegetation index (EVI) and soil-adjusted vegetation index (SAVI)) for discriminating mature rubber plantations from the high vegetation density [5]. Another study used SAVI, EVI, and NDVI in Kedah, Malaysia to determine different stages of rubber trees, and it concluded that some remained misclassifications might cause under- or over-estimation [6]. The study applied the NASA Landsat GeoCover product by developing NDVI and tasseled-cap transformation for the Mahalanobis Typicality classifier. They claimed that well-matching with provincial statistics for mature and middle-age rubber tree growth areas. The estimation of young rubber tree areas was difficult for performing this method to coarse resolution satellite data. Improvements could be produced to map young rubber trees more accurately with intensive high-quality training information [7]. Moreover, the investigation extended their applications to Southeast Asia by using Moderate Resolution Imaging Spectroradiometer (MODIS Terra) time-series NDVI data, and it claimed that the earlier problem was successfully overcome [8]. In Mindanao island of Philippines, the six bands of Landsat 8 OLI data and satellite-derived indices Tasseled Cap (Brightness, Greenness and Wetness), the Wetness-Brightness Difference Index (WBDI), NDVI and the Normalized Difference Structure Index (NDSI) were used to classify rubber tree plantations by using Mixture Tuned Match Filtering (MTMF) method. The results indicated the capability of the method to differentiate young from mature rubber plantations, with an overall accuracy of 73% [9]. In China's Xishuangbanna Prefecture, where a tropical forest is abundant, the forest areas were converted to rubber plantations during the period of booming rubber prices. The Land use change detection analysis was conducted to detect vegetation change of the other vegetation types large proportion transformed to rubber plantations by using Landsat 7 ETM+ and SPOT images acquired at different times [10]. Regarding a tremendous conversion of natural forests to rubber tree plantations in China's Xishuangbanna Prefecture, another study applied multi-temporal Landsat images (acquired in 1989, 2000, and 2013), producing overall accuracy over 80% [11]. Attempting to distinguish forests from rubber plantations, the integration of vegetation indices time-series and rubber tree phenological attributes was conducted to rapidly estimate plantation areas. [12] identified two phenological periods of rubber trees: 1) during the leaf abscission period in late February–March; and 2) during the new leaf emergence period in late March–April. Differences in vegetation indices were found to distinguish rubber plantations from forests. In addition, many approaches attempted to differentiate different stages of rubber plantations by using Radar imagery because of its cloud penetrability, many of which reported success [13] [14] [15]. However, very high cost-effectiveness was the disadvantage for performing to a very large areas of the global level planning.

Most digital image processing is mainly based on colours represented by values of digital numbers in each pixel combined into images. Timely monitoring using satellite data for the stages of rubber plantations has been less available in Thailand [7]. The Geo-Informatics and Space Technology Development Agency (GISTDA) provided financial support to map tapped rubber plantation areas for the entire country based on Landsat8 OLI [16]. The goal was to estimate the rubber latex yield to compensate the farmer's grant because of the decline in rubber prices since 2012. The study applied the on-screen digitizing method to delineate the tapped rubber plantations by using low- resolution image of this method, the tapped rubber tree plantations (> 7 years old) were still easily confused with the high vegetation density areas such as evergreen forest and very dense deciduous forest. Moreover, the confusion between other stages of rubber plantations and other Land Cover/Land Use (LCLU) types was encountered when using traditional PBIA approach, e.g., between young age rubber trees with intercropping and field crops and paddy fields with herbaceous plants; and between middle-age rubber tree plantations and the moderate vegetation density areas.

The satellite technology has been continually developed with increasing spatial resolution remote sensing imageries for supporting a detailed landscape mapping and local land-use planning. However, a speckle or "salt and pepper" disadvantage was generally found when the traditional PBIA was applied to very high-resolution images. With this problem contributed to the inaccuracy of the PBIA classification [17] [18], it has been completely overcome by the use of Object-Based Image Analysis (OBIA) to segment image objects based on both spectral and spatial characteristics [19] [20]. A commercial software package for OBIA was made available in 2000, and research into the use of OBIA has highly increased in a number of applications, particularly for high-resolution satellite data [21].

There have been numerous research studies comparing traditional PBIA and OBIA classification for LCLU application. The study confirmed that application of OBIA had a superior performance than PBIA for urban landscape classification using QuickBird data, with the high overall accuracy of 90.40 % [22]. The high accuracy was found as using OBIA for urban land use applying to both medium and high spatial resolution imageries with an overall accuracy of 77.90% and 85.65%, respectively [23]. Moreover, the application of multi-spectral GeoEye imagery for urban tree species mapping confirmed that OBIA was significantly better than PBIA [24]. OBIA has been compared to PBIA for supporting LCLU change analysis. The study reported the potential of OBIA for extracting land cover information from ASTER data with an overall accuracy of 78.5%. The resulting map has improved on capturing over spatially heterogeneous land covers of tropical Australia [25]. For LCLU mapping in Selangor, Malaysia, spectral bands of SPOT 5 data were applied, and OBIA was used to compare with PBIA. The result indicated that overall accuracy of OBIA classification was higher than PBIA [26]. The mapping of salt cedar using QuickBird imageries with multi-scale OBIA, which employed spectral, texture and shadow features, produced a high overall accuracy of 91.6% [27].

With the rapid expansion of rubber tree plantation in northeast Thailand, the application of a very high resolution image processing and OBIA to distinguish rubber plantations was critical for estimating their proportion of land use within and between international borders. Moreover, the stand age class of rubber tree plantations information was important for supporting watershed land-use planning in term of economic and environmental

analysis. Therefore, the minimizing of confusion between rubber tree plantations and other mixed and diverse ground cover conditions, including forest areas via the integration of OBIA with satellite derived indices, image texture, plant phenology, and field observations was the goal of our study. We applied THAICHOTE satellite data as well as intensive ground observation for training areas to model and digitally devise a synergistic approach to distinguish different stages of rubber plantations and aggregate OBIA, plant phenology and satellite-derived indices. With this study, we expected to rapidly increase and enhance the mapping of rubber plantations with higher accuracy. The obtained results could be used to encourage farmers to use attractive, highly priced crops as viable land use alternatives.

2. STUDY AREA

The study area is in the northeasternmost region of Thailand and a portion of the Lao People's Democratic Republic (Lao PDR) (Fig. 1) between latitude 18°00' to 17°46'N and longitude 104°08' to 104°12'E; the study area covers much of the province of Nakhon Phanom, including part of Bueng Kan. The uppermost boundary is the Mekong river, which shares the border with the province of Bolikhamsai of the Lao PDR. The study area covers an area of approximately 36,856 ha, with elevations between 130 and 550 m above mean sea level [28].

The climate is tropical monsoon with a mean annual rainfall of approximately 2,340 mm [29], most of which is distributed from May to October. The region is among the areas affected by tropical cyclones from the South China Sea in the period of August to October, with the intensity of tropical storms or higher that bring more and heavier rains. The gently undulating topography of a continuously alternating surface of uplands and lowlands, and some prominent hills characterize the landscape in the region. The areas are drained southeastwards to the Mekong by numerous creeks (Huai Langka, Huai Sai, Nam Mao, Huai Kathat). Soils are inherently low in fertility, have coarse to medium texture and were formed from alluvium with a high proportion of sandy materials. Most of the soils are Typic Ustifluvents, Aeric Kandiaquults, Plinthic Paleaquults and Typic Plinthustults [30] [31]. Traditional agriculture is cassava, sugarcane, and orchards for upland well-drained soils and rice for flat lowlands. The bund-paddy field in association with sparse trees and rubber stand plantation dominate the land use and

land cover in the area. The native forest patches of dry dipterocarp and mixed deciduous and evergreen types are also found. Rubber trees were not historically planted in this region. Moreover, the rubber plantations replace the traditional field crops and the ecologically native forest, which has led to forest fragmentation. To date, most rural households are engaged in rubber production and paddy rice, which generates inconsistent incomes because of the highly volatile market prices [32] [33]

3. MATERIALS AND METHODS

In this study, we used cloud-free, multispectral and panchromatic THAICHOTE data (formerly known as Thailand Earth Observation System-THEOS) acquired after the rainy season. For image pre-processing, the data were transformed to top-of-atmosphere (TOA) radiance and geometric correction was performed. The eCognition developer package [34] was applied for OBIA. Two levels of classification based on OBIA approach were performed. At the first level, the four different subsets of Vegetation Canopy Density (VCD); high VCD, moderate VCD, low VCD, and very low VCD were classified using the integration of multi-scale image segmentation, the association of NVDI with BI, and intensive training areas. At the second level, the rubber plantation areas derived from each of four subsets were next classified to discriminate stand age class of rubber plantations from other LCLU types with a particular approach and a range of different approaches. Several exemplars of the field survey for gathering information about LCLU rubber tree stand age and geographical characteristics were observed. The information obtained was used for the identification of training sets and some were set aside for output validation. Figure 2 shows the flowchart of the study. Details of the methodological procedure are as follows.

3.1 Image Selection

The THAICHOTE satellite, launched in October 2008, was Thailand's first Earth observation satellite and had the objective of resource management and mapping in Thailand and around the world. The characteristics of the THAICHOTE satellite are shown in Table 1. In this study, we used the panchromatic, pansharpened and multi-spectral image set acquired on December 15th, 2012, including the multispectral band on February 8th, 2011, which was the period of flushing rubber tree leaves [35] [36].

3.2 Pre-Processing

To normalize the THAICHOTE data, digital values of the selected images were transformed to TOA radiance based on the method developed by [37] using raster calculation in PCI Geomatica 2014, which the exo-atmospheric solar irradiance, the Earth–Sun distance, and the solar zenith angle are required. The THAICHOTE image scenes were then transformed to the world geodetic system 1984 (WGS84) coordinates using ground control points (GCP) from the 2002 aerial orthophotography and the nearest neighbour resampling method. Then, the areas of water bodies were excluded using Near Infrared. Additionally, panchromatic and multi-spectral bands acquired in December 2012 were used to create pansharpened images using the automatic image fusion algorithm [38] available in PCI Geomatica 2014 developed by PCI Geomatics Ontario, Canada.

Table 1: The Characteristic of THAICHOTE Satellite Data.

Characteristics	Capabilities
Bands	Panchromatic: 0.45 - 0.90 μm B1 (Blue): 0.45 - 0.52 μm B2 (Green): 0.53 - 0.60 μm B3 (Red): 0.62 - 0.69 μm B4 (Near infrared): 0.77 - 0.90 μm
Spatial Resolution	Panchromatic 2 m Multispectral 15 m
Swath width	Panchromatic: 22 km at Nadir Multispectral: 90 km at Nadir
Repeat cycle	26 days

3.3 Image Segmentation and Vegetation Canopy Density *(VCD)* Subset Extraction

For this stage, the eCognition developer package was used for OBIA. The VCD map was generated through the integration of multi-scale image segmentation, the association of NDVI with BI, and intensive training areas. Image segmentation is the importantly first step for dividing the image set into objects or regions with different spectral and spatial characteristics. The multiresolution segmentation was used, which algorithm required shape, compactness, band layers and scale parameters to derive meaningful image objects. Trials of shape factors were tested and iterated within a factor of 0.3 to 0.7 because of homogeneous, large, and more obvious regions of the rubber plantation areas. As a result of the trials, we set the shape factor to 0.4 as an appropriate value. The shape and color balance led to a color

factor of 0.6; the lower the shape value, the greater the impact of color on the segmentation process. Moreover, given a similar trial procedure for the compactness factor, its value was set to 0.6, which provided a smoothness factor of 0.4; the greater the compactness value, the more compact the objects. In this operation, we defined band layer weights of 1, 1 and 2 for B2, B3, and B4, respectively. Paying attention to scale is more important to multiresolution segmentation, and estimates of the scale parameter 2 (ESP-2) Tool [39] generated a relationship between the local variance (LV) and scale by which the rate of change for the scale could be computed (Fig. 3). The peaks in the rates of change provided the scale levels at which the image set could be segmented for the multi-scale segmentation process. The first, second and third scale level selected were adopted to the image sets with 31, 71 and 126 for fine, moderate and coarse image objects, respectively (bold vertical dashed line in Figure 3).
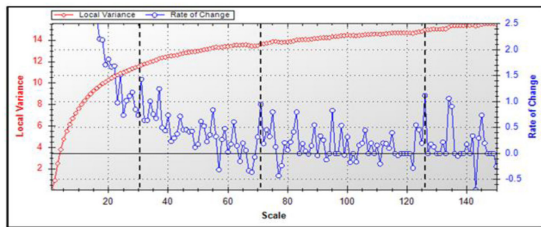

Figure 3: Estimation of the scale parameter.

At the same time, the establishment of VCD using the multispectral band was executed by defining a fusion of NDVI [40] and BI [41]. This relationship was obtained from the mean vector and the standard deviations of training areas. Since emphasis was placed on the rubber tree plantation areas, the classifiers required the presence of the other class information. Sufficient training sites required both the rubber tree plantation areas and other classes. The training areas totalled 620 sites (Table 2) and came from ground observation via field surveys and set asides to not only understand LCLU types but also for further verification of the classification.

Figure 4 shows a map of the ground observations for the training areas. Ground observations were financially supported by GISTDA under the project on the development of a landowner database for rubber plantations using THAICHOTE satellite imagery. The combination of NDVI and BI was then developed to intimately incorporate with the objects. The high values of NDVI are associated with low values of BI, and high VCD is an association of high NDVI and low

BI values. In contrast, lower VCD values are attributed to the highest BI values with much smaller NDVI values; such a combined value was set as bare fallow land or built-up areas. The formulas for computing the BI and NDVI are as follows:

$$NDVI = \frac{B3 - B4}{B3 + B4} \quad (1)$$

$$BI = \sqrt{\frac{B2^2 + B3^2}{2}} \quad (2)$$

where B2 is TOA reflectance in the green band (0.53 - 0.60 μm), B3 is TOA reflectance in the red band (0.62 - 0.69 μm) and B4 is TOA reflectance in the near infrared band (0.77 - 0.90 μm)

An interval of generated VCD values was then classified into four subsets (Fig. 5) based on the Jenks Natural Breaks Classification, which assigns data to optimize the arrangement of a set of values into "natural" classes. This is done by seeking to minimize the average deviation from the class meanwhile maximizing the deviation from the means of the other groups [42]. In this study, the VCD was input into image objects to develop four subsets with fine-scale of 31 for high VCD and moderate VCD regions, moderate-scale of 71 for low VCD regions and coarse-scale of 126 for very low VCD regions. Details of each VCD subset, which consist of the rubber tree plantation areas and their confusion, are provided in Table 3. The photographs of different age rubber trees and other land cover and land use types were shown in figure 6. The four VCD subsets that resulted from the first level classification were further processed to differentiate the rubber tree stand ages of the plantation areas.

Table 3. The possible confusion within VCD subsets.

VCD Subsets	Confusion
High VCD	MatureR)rubber trees > 7 years(, VDF
Moderate VCD	MidR)rubber trees 4-7 years(, MDF, PerennialC, FC
Low VCD	YoungR)rubber trees 1-4 years(, Paddy, FC, DF, Built up
Very low VCD	SaplingR)rubber trees < 1 years(, FLpaddy

3.4 Rubber tree stand age and LCLU classification

The aim of analysis within high VCD was to distinguish MatureR (rubber trees > 7 years)

from other high VCD. High VCD regions, as described in Table 3, had confusing areas among MatureR and very dense forest (VDF), mostly dense forest types that were substantially covered by uneven layers of canopy of over 4 stories and that showed coarse texture in the images. The canopy of MatureR had even crowns and completely covered the ground surface with the crown length is over 10 m. The understory of MatureR was relatively sparse wild plants and herbaceous plants, with mostly bare soil because of light interception and being trampled underfoot for rubber tapping. In high VCD regions, the December 15th, 2012 multispectral image had confusion between the MatureR and the other plants. The MatureR trees typically flush their leaves during February, whereas no common occurrence of leaf shedding was found for young rubber trees. Therefore, the mean of NDVI features of THAICHOTE for December 15th, 2012 and February 8th, 2011 were used to investigate class separability. The 41 exemplars each for the leaf flushing and VDF areas were applied (Table 4), which resulted in NDVI values that provided threshold sets of two date images. Applying the membership function classifier [22], which is the interval of the NDVI values as threshold sets, determined the MatureR class. The MatureR areas that shed their leaves could be delineated and differentiated from the VDF within high VCD regions.

Table 4: Training and test sites use in High VCD, Moderate VCD, Low VCD, and Very low VCD regions.

VCD Subsets	LCLU Class	No. of training areas
High VCD	Rubber tree plantations > 7 years (MatureR)	41
	Very Dense Forest (VDF)	41
	Total	82
Moderate VCD	Rubber tree plantations 4-7 years (MidR)	58
	Moderately Dense Forest (MDF)	24
	Perennial crops and orchard (PerennialC)	19
	Field crop and herbaceous plants (FC)	28
	Total	129
Low VCD	Rubber tree plantations 1-4 years (YoungR)	31
	Paddy fields (Paddy)	19
	Field crop and herbaceous plants (FC)	17
	Degraded forest (DF)	25
	Urban and Built up areas (Built up)	15
	Total	107
Very low VCD	Rubber tree plantations < 1 years (SaplingR)	70
	Fallow bare land and paddy field (FLpaddy)	62
	Total	132

For moderate VCD regions, differentiating a range of the MidR (rubber trees 4-7 years) areas from the other moderate VCD was the purpose of this stage, in which a decision tree for classification using the classification and regression tree (CART) approach was performed. The MidR had an intercrown spacing of approximately 40-70%, which means sky visibility from a point beneath with the appearance of rows of trees. The plantations usually had confusion with MDF, DF, PerennialC, and FC. Ground observations of locational areas of a total of 129 training areas (Table 4) were accomplished. The input features for CART decision tree classifier were defined using feature space optimization (FSO tool) [34] [43], which determined 12 spectral, 7 shape, and 12 texture features (Table 5). Based on the eCognition nearest neighbour classification, FSO tool assessed the Euclidean distance in feature space between the training exemplars, which produced the best class separation distance by the largest of the minimum distances between the least separable classes [34]. The feature combination providing the best class separation distance was chosen for CART classifier, which available in eCognition. The CART model was created based on the attribute information attached to the training segments, which resulted in the MidR and others.

Table 5: Input Features.

Category	Object Feature
Spectral	Mean B1, Mean B2, Mean B3, Mean B4, Mean BI, Mean NDVI Standard deviation (Std.) B1, Std. B2, Std. B3, Std. B4, Std. BI, Std. NDVI
Shape	Asymmetry, Border index, Compactness, Elliptic fit, Rectangular fit, Roundness, Shape index
Texture	Grey-level co-occurrence matrix (GLCM) Homogeneity (all dir.) PAN, GLCM Contrast (all dir.) PAN, GLCM Dissimilarity (all dir.) PAN, GLCM Entropy (all dir.) PAN, GLCM Ang. 2nd moment (all dir.) PAN, GLCM Mean (all dir.) PAN, GLCM Std. (all dir.) PAN, GLCM Correlation (all dir.) PAN, Grey-level difference vector (GLDV) Ang. 2nd moment (all dir.) PAN, GLDV Entropy (all dir.) PAN, GLDV Mean (all dir.) PAN, GLDV Contrast (all dir.) PAN

For low VCD, the aim of the stage was to discriminate confusion between YoungR plantations (rubber trees 1-4 years) associated with intercropping and herbaceous from the other low

VCD cover type. Regarding table 3, this stage plantation usually had confusion with Paddy, FC, DF, and Urban Build up areas. The method used for low VCD was similar to that for moderate VCD. A total of 107 exemplars comprised the class, as depicted in Table 4. Other procedures were accomplished the same as for moderate VCD.

For very low VCD region, which dominated by a very low VCD and the highest brightness areas. The rows of SaplingR (rubber saplings newly planted < 1 years old) were easily observed in contrast with more obvious bare land, as seen from the THAICHOTE panchromatic image (2 m resolution). The rows of rubber saplings were distributed equally, with a row spacing of 7 m, and we found fallow bare lands and paddy fields (FLpaddy) in addition to SaplingR. We tried to discriminate the SaplingR and the FLpaddy. The GLCM entropy texture algorithm was then applied to distinguish the SaplingR from FLpaddy. The value for entropy was high in the case of equal distribution of the rows of trees. We used the GLCM entropy formula as follows:

$$Entropy = \sum_{i,j=0}^{N-1} Pi, j(-\ln Pi, j) \qquad (3)$$

where i is the row number, j is the column number, Pi,j is the normalized value in the cell i, j and N is the number of rows or columns.

A total of 132 exemplars were found within very low VCD regions (Table 4), which consisted of rows of SaplingR and FLpaddy areas. Those two classes were separated by their interval values coming from the exemplars. The values of the training set for the SaplingR class were theoretically higher than those of the FLpaddy. The membership function with the interval of threshold sets achieved was analysed to assign the class

3.5 Validation

For validation of rubber tree stand age and LULC classification within high VCD regions, we used the reference areas (mature rubber) using the on-screen digitizing method with intensive ground observations conducted by GISTDA; the classified image acquired from image differencing used periods of defoliation in February 2011. High VCD regions were divided into cells with four-square kilometer grid spacing. Then, random of the number of grid cells was carried out for comparison made between referenced and estimated areas to generate error percentage (% ERROR), root mean square error (RMSE) and relative RMSE with the referenced area as well as a correlation between the

reference and the estimate. The formulas for computing the error percentage and RMSE are as follows:

$$\%ERROR = \left(\frac{Estimate - Reference}{Refference} \right) * 100 \qquad (4)$$

$$RMSE = \sqrt{ \frac{\sum_{i=1}^{n} (Reference - Estimate)^2}{n} } \qquad (5)$$

where n is the number of grid cells in the study area.

To validation of rubber tree stand age and LULC classification within moderate VCD and low VCD regions, the output map was checked against the ground observations for a total of 243 sites set aside for validation. Of the total sites, 96 and 147 exemplars were intensively recorded for LCLU types present in moderate VCD and low VCD regions, respectively. Dispersion of the sites throughout the scene increased the chance that they were representative of all the LCLU types present in the scene (Fig. 7). Observations used to ensure reliable exemplars included rubber tree age, diameter at breast height, rubber tree stand height, visible VCD, understory plants, and others. A confusion matrix between the output map and the ground observations was created to compute the accuracy of users and producers and the overall accuracy as well as the Cohen's kappa coefficient [44] [45]. The validation procedure for very low VCD was similar to that of high VCD because there were two LCLU categories to compare.

4.   RESULTS AND DISCUSSION

4.1 Vegetation Canopy Density (VCD) Subsets Extraction

A map of VCD subsets is shown in Figure 8. Table 6 compares the areas of each subset; the areas of high VCD, moderate VCD, low VCD, and very low VCD covered 30.15%, 25.03%, 31.59% and 8.68%, respectively. Each of the subsets was spectrally confused with other LCLU types as was previously stated.

The distribution of the rubber plantation areas predominantly replaced the traditional crops (cassava and sugarcane), degraded forest and some forest reserves. More importantly, the study applied multi-scale image segmentation to delineate the different of VCD subsets, corresponding to fine, moderate and coarse regions, depending on the

spectral heterogeneity. The fine-scale parameter allowed heterogeneity and small objects that corresponded to the image objects of high VCD and moderate VCD regions. The coarser scale provided more homogeneity and large objects. The values of the scale parameter produced variation in the size of image objects. The largest objects were then produced for very low VCD. This study mainly corresponded to many authors who stated that the multi-segmentation is initially required before classify image objects into LCLU classes [46] [47] [48] [49], with this procedure have made more increase accuracy for LCLU mapping with very high resolution satellite data. The multi-scale image segmentation was performed to establish three-level hierarchical image object for tree species classification at the finest level of IKONOS data with the high overall accuracy of 90 % [50] and 80 % for Quickbird data [51]. In the other hand, [52] have performed OBIA single-level image segmentation for rubber tree stand ages mapping by using SPOT-5 imagery. They suggested that the intensive and effective of training areas from expert systems should be taken for more accurate.

So far, we remained unable to discriminate the rubber plantations from other plants, and the MatureR (rubber trees > 7 years), MidR (rubber trees 4-7 years), YoungR (rubber trees 1-4 years) and SaplingR (rubber trees < 1 years) areas shared portions within high VCD, moderate VCD, low VCD, and very low VCD regions, respectively. As a result, this analysis used the association of NDVI with BI and multi-scale image segmentation for the first level to extract the distinctive characteristics of each region (Fig. 9)

Table 6: Areas of vegetation canopy density subsets for the study areas.

VCD Subsets	Areas	
	Ha	**Percentage**
High VCD	11,111.20	30.15
Moderate VCD	9,223.39	25.03
Low VCD	11,641.80	31.59
Very Low VCD	3,200.17	8.68
Water body	1,679.87	4.56
Total	36,856.43	100.00

4.2 MatureR (rubber trees > 7 years) classification within high VCD regions.

The values of the December 2012 NDVI were different from those of February 2011 because the tapped mature rubber trees shed their leaves, and the confusion between MatureR and other plants could be resolved by the NDVI differencing of the two dates. Figure 10 shows a comparison

between NDVI values for the two date images created from the values of their means and standard deviations. Significant differences in the NDVI values were found. Note that MidR trees do not flush their leaves like MatureR trees. The MatureR areas are clearly distinguishable based on NDVI image differencing.

Moreover, a comparison between the referenced and estimated areas was made (Table 7); the highest error percentage was found in the grid ids 1 and 19, whereas most of the areas in other grid ids were relatively low: RMSE was 39.49 and RMSE/Reference was 0.92%. The referenced and the estimated areas were well correlated, with R^2 = 0.92 (Fig. 11). Results from this analysis were reliable for distinguishing MatureR from very dense forest (VDF).

Table 7: Comparison between the referenced and estimated areas for mature rubber plantations within high VCD regions.

Grid ID	Reference (ha)	Estimate (ha)	% Error
1	27.70	48.20	74.01
2	176.75	157.22	-11.05
3	314.55	234.38	-25.49
4	267.21	291.81	9.21
5	70.85	109.57	54.65
6	314.81	232.74	-26.07
7	512.14	405.58	-20.81
8	585.11	526.25	-10.06
9	31.16	29.72	-4.63
10	160.82	168.80	4.96
11	196.94	262.21	33.14
12	437.27	416.23	-4.81
13	166.31	246.69	48.33
14	107.21	112.34	4.78
15	331.57	313.02	-5.60
16	223.46	202.67	-9.30
17	21.91	23.74	8.31
18	139.31	121.41	-12.84
19	109.33	185.74	69.89
20	62.27	82.89	33.12
21	47.25	67.32	42.47
Total	4,303.94	4,238.54	
RMSE	39.49		
RMSE/ Reference(%)	0.92		

The distribution of MatureR (rubber trees > 7 years) is depicted in Figure 12. Areas of MatureR and the VDF accounted for 5,148.13 and 5,963.07 ha, respectively, representing 46.33% and 53.67% of high VCD areas. Additionally, selection of the defoliage month (February image) was very difficult and sometimes not available because of cloud cover for applied to THAICHOTE data. In this study, we prefer to apply the February 2013

image instead of the February 2011 image. The comparison between only two dates of NDVI is the drawback of this study. Another study used temporal resolution potential of Landsat and MODIS imageries to support rubber tree phenological information with nearly 80 % of overall accuracy [53]. Moreover, using Landsat NDVI times series incorporated with PBIA and OBIA approach produced the high overall accuracy of 87 % [54]. However, a potential of spatial resolution of THAICHOTE data should be integrated with the temporal resolution of Landsat data for more accuracy for MatureR classify within high VCD regions. Regarding the monoculture rubber tree planted with equal for spacing and single crown of MatureR led to presented specially of pattern and smooth textural contextual, which different from coarse texture classes of very dense forests with high crown density. Therefore, this method should be improved by using texture image analysis conducted by [55] for supporting the multi-scale image segmentation approach.
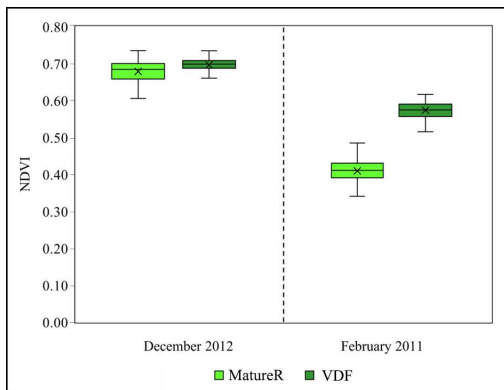
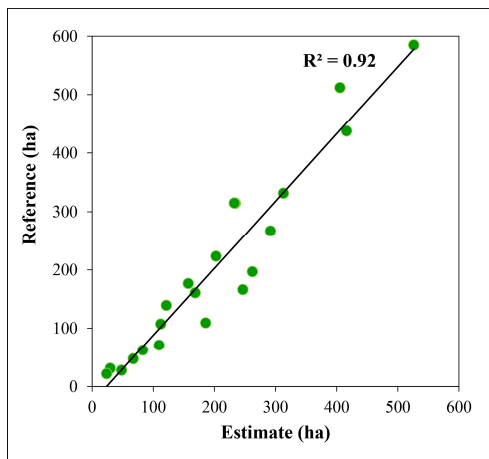*Figure 10: The values in NDVI between two date images.*

Figure 1 1 : Correlation between the reference and the estimated areas within High VCD.

4.3 MidR (rubber trees 4-7 years) classification within moderate VCD regions.

We defined 31 features to be applied for feature optimization for moderate VCD analysis. After compilation of selected features, the FSO tool selected 21 features for CART decision tree classification (Table 8); the features consisted of 11 layer values, 5 geometry, and 5 texture features. The result of minimum class separation distance for the aggregation of features was 0.798151 (Fig. 13). Table 9 shows the separation distance matrix of the best dimension for moderate VCD and the minimum values of the separation distance between the pairs of LCLU types. The separation distances of the MidR (rubber trees 4-7 years) between other LCLU types were 1.073848, 1.052242 and 0.798151 for FC, MDF, and PerennialC, respectively.

Table 9: Separation distance matrix used to evaluate the best dimension for moderate VCD.

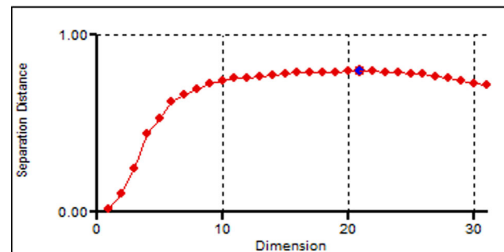| Class/Class	MidR	FC	MDF	PerennialC
Dimension 21				
MidR	0.000000	1.073848	1.052242	0.798151
FC	1.073848	0.000000	0.969085	1.739538
MDF	1.052242	0.969085	0.000000	1.380219
PerennialC	0.798151	1.739538	1.380219	0.000000

Figure 13: Distance of each Dimension for distinguishing MidR within moderate VCD regions.

Inputs for the CART decision tree classifier comprised 21 features and training objects as defined and resulted in the classification of LCLU types present in moderate VCD regions. Of the 21 features selected, only 5 features were selected and used by the CART model to estimate class membership of the training objects. These were GLDV Entropy (all dir.) PAN, GLCM Entropy (all dir.) PAN, Mean NDVI, Shape index and Std NDVI. Figure 14 represents the output CART model generated by the analysis process. The five features and associated thresholds are shown, each split into the classes in accordance with the threshold of the features used. As a result,

we could differentiate the MidR from other LCLU types.

The areas of MidR covered 1,546.74 ha, 16.77% of the moderate VCD regions (Table 10). The distribution of MidR is depicted in Figure 15. The drawback of this method is that many input features are used, particularly for inexperienced researchers. However, the study conducted by [56] used both layer values and texture features of over 50 inputs to OBIA combined with the CART decision tree to classify arid land vegetation with QuickBird imagery. With regard to the feature optimization by which GLDV Entropy and GLCM Entropy were selected for CART classifier. It can reflect the pattern of MidR having rows spacing of rubber stands.

This study applied multi-resolution segmentation to determine the optimal scale, whereas our study adopted ESP-2 tools to set up the optimal scale. It should be observed that we used TOA reflectance, which has relatively low values and resulted in lower values of separable distance. However, the class separability was reliable as is described in the validation below (Table 14a). The performance of OBIA integrated with multi-scale segmentation, feature optimization, and CART decision tree classifier to discriminate MidR between other LCLU type produced high overall accuracy about 84 %. Our study used a combination of layer values, texture, and geometry features for CART model, which different to another study using of only vegetation indices features for decision tree classifier with overall accuracy for 80 % [52].

Table 10: Areas of the MidR and other cover classes.

Classes	Areas	
	Ha	Percentage
MidR (rubber trees 4-7 years)	1,546.74	16.77
FC	1,963.23	21.29
MDF	5,511.37	59.75
PerennialC	202.05	2.19
Total	9,223.39	100.00

4.4 YoungR (rubber trees 1-4 years) classification within low VCD regions.

For low VCD regions, YoungR (rubber trees 1-4 years old) was confused with other LCLU types such as Paddy, FC, DF, and Build up areas. The approach to the study method for low VCD was similar to that of moderate VCD. Differences in scale, input features and separation distance were obtained, yielding the moderate segmentation scale objects of 71 and 22 input features and a separable

distance of 1.081108 for distinguishing YoungR and other LCLU types within low VCD regions (Fig. 16). The 22 input features consisted of 11 layer values, 4 geometries and 7 textures (Table 11). Table 12 shows the separation distance matrix of the best dimension and the minimum values in the separation distance between the pairs of LCLU types for distinguishing YoungR and other LCLU types. The separation distances of YoungR between other LCLU types were 2.092412, 1.542968, 2.074776 and 2.256650 for Paddy, FC, DF and Built up, respectively. It should be noted that the six features consisting of GLDV Entropy (all dir.) PAN, Std Green, Border index, Mean Red, GLCM Correlation (all dir.) PAN and Mean NDVI were appropriate for YoungR. The output CART model established is shown in Figure 17.

Table 12: Separation Distance Matrix of the best dimension for distinguishing YoungR within low VCD regions.

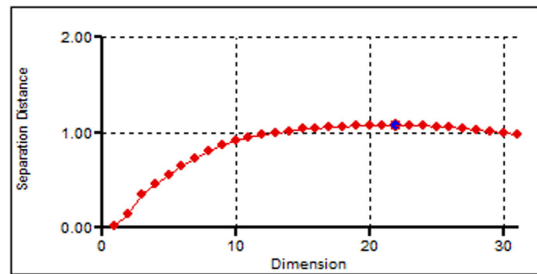| Class/ Class	YoungR	Paddy	FC	DF	Built up
Dimension 22					
YoungR	0.000000	2.092412	1.542968	2.074776	2.256650
Paddy	2.092412	0.000000	1.081108	1.211804	2.700310
FC	1.542968	1.081108	0.000000	1.352151	4.075604
DF	2.074776	1.211804	1.352151	0.000000	3.179920
Built up	2.256650	2.700310	4.075604	3.179920	0.000000

Figure 16: Distance of each dimension for distinguishing YoungR within low VCD regions.

It should be noted that the border index which provided the ratio between the border lengths of the image object and the smallest enclosing rectangle was also used in CART classifier. The index helps discrimination YoungR from built up and paddy land. The distinction between YoungR and other LCLU types is evident. These areas covered 1,729.97 ha, which accounted for 14.86% of low VCD. Paddy had the largest area found within low VCD regions (Table 13). A map showing the different classes within low VCD regions is illustrated in Figure 18.

Accuracy assessments of image-based classification against field-based observations within moderate VCD and low VCD regions created cross tabulation table are shown in Table 14(a) and (b). The validation results obtained Cohen's kappa coefficient about 0.78 and 0.80 for LCLU classification within moderate VCD and low VCD, respectively. The accuracy shows high-reliability user's accuracy of 81 % for discriminating MidR from other LCLU types (Table 14a) and 83 % for distinguishing YoungR within low VCD regions (Table 14b). Additionally, the user and producer accuracies for all LCLU classes differentiation were highly satisfactory. We can conclude that the differentiation of the MidR from the other low VCD cover type was successfully achieved with the method studied and that YoungR could be resolved from the other classes.

Table 13: Areas of YoungR and other LCLU types.

LCLU Classes	Areas	
	Ha	**Percentage**
YoungR (rubber trees 1-4 years)	1,729.97	14.86
Paddy	4,012.93	34.47
FC	3,195.67	27.45
DF	1,902.27	16.34
Built up	800.96	6.88
Total	11,641.80	100.00

Table 14: The agreement between image-based classification and field-based observations within moderate VCD and low VCD regions.

(a) Moderate VCD							
Image based classification	**Field based observation**					**Accuracy (%)**	
	MidR	**FC**	**MDF**	**PerennialC**	**Total**	**UA**	**PA**
MidR	29	2	3	2	36	80.56	87.88
FC	0	24	1	0	25	96.00	85.71
MDF	3	2	22	1	28	78.57	84.62
PerennialC	1	0	0	6	7	85.71	66.67
Total	33	28	26	9	96		
Overall accuracy (%)			84.38				
Cohen's kappa coefficient			0.78				

(b) Low VCD							
Image based classification	**Field based observation**					**Accuracy(%)**	
	YoungR	**Paddy**	**FC**	**DF**	**Built up**	**Total**	**UA**	**PA**
YoungR	33	2	3	1	1	40	82.50	86.84
Paddy	1	26	2	1	0	30	86.67	81.25
FC	2	2	27	2	1	34	79.41	84.38
DF	0	2	0	18	0	20	90.00	78.26
Built up	2	0	0	1	20	23	86.96	90.90
Total	38	32	32	23	22	147		
Overall accuracy (%)				84.35				
Cohen's kappa coefficient				0.80				

Regarding the possible confusion within moderate and low VCD subsets in table 3 and

figure 5, detailed the confusion between LCLU classes more than two categories due to the mixed-pixels problems occurred within these VCD subsets such as herbaceous plants and field crops as planted intercrops within YoungR and MidR plantations. The stand age rubber tree plantations OBIA analyzed within moderate VCD and low VCD regions should be improved by the other classifier such as Support-Vector Machine (SVM), Mahalanobis, and K-Nearest Neighbour (K-NN), these classifiers were found that rather providing higher performance than decision tree classifier [52]. Moreover, the Leaf area index (LAI) and the Land Surface Water Index (LSWI) should be used to distinguish MidR from oil palm and other vegetation [57].

4.5 SamplingR (rubber trees < 1 years) classification within very low VCD.

Most of the areas under very low VCD were associations of the rows of SaplingR newly planted rubber trees in 2012 and FLpaddy as shown in Figure 19. We applied the GLCM Entropy (all dir) PAN for SaplingR discrimination within very low VCD, which was not texturally uniform; very large entropy was found for the rows of SaplingR values and lower entropy for FLpaddy. The two LCLU types were distinguishable (Fig. 20), with close values in the BI of SaplingR and FLpaddy but a significant difference in GLCM Entropy (all dir.) PAN. Approximately less than 5% of the overlap between the two LCLU types was observed. This overlap area exhibited some herbaceous plants present in both LCLU types. For the threshold values, the values in GLCM Entropy (all dir) PAN was calculated and the values higher than 7.70 were assigned to SaplingR, whereas the lower values were FLpaddy.
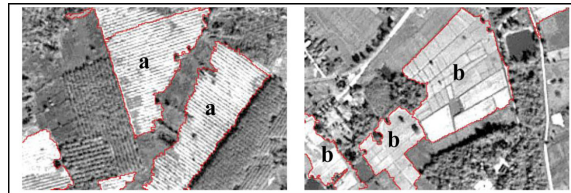

Figure 19: Panchromatic image showing a) the rows of rubber sapling plantations and b) the fallow bare lands and paddy fields.

The diverse ground conditions of vegetation, intercropping and herbaceous plants and bare soil within a newly planted rubber tree plantations were discussed by [7] [12] that mixed-pixels problem within a non-closure canopy cover

of young rubber tree plantations lead to the difficult for rubber tree plantation stand age mapping. The coarser segmentation scales level produced decreasing of segmentation accuracies [58]. However, our study has presented the advantage of multi-scale image segmentation and selecting at the coarse scale for very low VCD subset. The image objects resulted were more fit pronounced to the brightness areas of SaplingR plantations contextual, which were obviously contrasted to more VCD higher of neighbor areas (Fig. 19a) and enabled paddy bunds to be a part of image objects within FLpaddy was shown in Figure 19b.
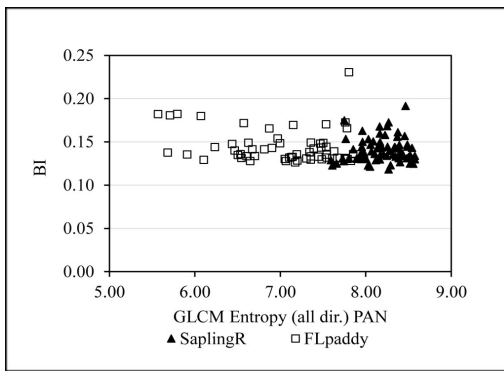
Figure 20: The relationship between BI and GLCM Entropy (all dir.) PAN for SaplingR and FLpaddy within very low VCD

Table 15: Comparison between the referenced and estimated areas for SaplingR within very low VCD regions.

| Grid ID	Reference (ha)	Estimate (ha)	% Error
1	40.86	54.19	32.63
2	41.78	46.76	11.93
3	75.62	117.99	56.03
4	155.54	182.01	17.02
5	95.00	86.06	-9.41
6	140.93	167.97	19.18
7	1.50	0.77	-49.09
8	89.82	109.72	22.16
9	92.69	137.68	48.54
10	121.94	154.65	26.83
11	97.90	135.23	38.13
12	17.24	34.22	98.54
13	51.76	82.37	59.15
14	120.38	185.49	54.09
15	40.47	50.70	25.26
16	30.49	46.42	52.24
17	6.28	11.07	76.40
18	39.56	73.65	86.16
19	19.00	23.39	23.12
20	17.85	30.83	72.69
Total	1,296.62	1,731.18	
RMES	22.80		
RMSE/ Reference (%)	1.76		
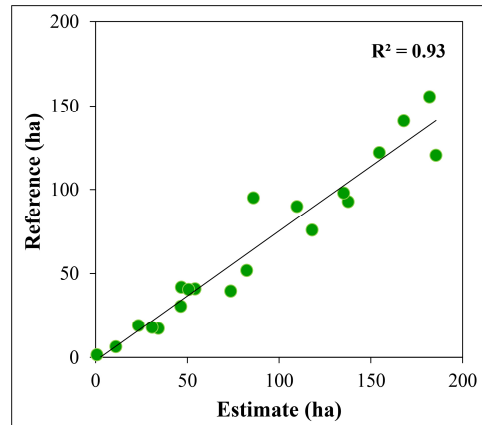
Figure 22: Correlation between the reference and the estimated areas within very low VCD regions.

The THAICHOTE rubber sapling map defined as less than one-year-old covered an area of approximately 70.69% of the totaled very low VCD regions, or 2,262.04 ha (Fig. 21). It is expected that the areas periodically decreased because of a decline in rubber prices that provoked stand logging on public land and more interest in traditional crops. The separability of the SaplingR from FLpaddy is clearly seen, with an RMSE of 22.80 with an RMSE/Reference of 1.76% (Table 15). The high correlation between estimated and reference areas was 0.93 (Fig. 22); however, a high error percentage in each of the grids may have been produced due to uncontinuous rows of unhealthy SaplingR and herbaceous plants present in some parcels. This is easily confused with FLpaddy which we can observe in field observation.

4.6 Different stages of rubber plantations map

Figure 23 shows the distribution of mature, middle-age, young and sapling plantations in the study area. The areas of mature, middle-age, young and sapling plantations as of 2012 covered 6.14, 4.69, 4.20 and 13.97%, respectively (Table 16). To date, the young and sapling rubber plantations can be tapped, mature rubber stands can be logged, and an agricultural extension programme has been promoted by the government to decrease the surplus of rubber production. In addition to the extension programme, reforestation in public lands was extended to reduce the plantations in support of the higher price of rubber products. Rapidly increasing of rubber tree expansions effects to decreasing of paddy fields low land, which is unsuitable marginal areas for rubber trees [4][58]. The precision of rubber tree stage classes spatial information has efficiency for supporting the decision of sustainable natural rubber production

[59] and the extension agriculture programs of government for determining production technology appropriated to each of stand age classes rubber tree plantations, for example, the intercropping extension program; rubber-cassava-rice or rubber-cassava intercropping systems for farmer higher income raising during the first 3 years old stand ages rubber trees [60].

Table 16: The areas of mature, middle, young and sapling-aged rubber tree plantations for the study areas.

Cover type	Area	
	Ha	**Percentage**
SaplingR	2,262.04	6.14
YoungR	1,729.97	4.69
MidR	1,546.74	4.20
MatureR	5,148.13	13.97
VDF	5,963.07	16.18
MDF	5,511.37	14.95
PerennialC	202.05	0.55
DF	1,902.27	5.16
FC	5,158.90	14.00
Paddy	4,012.93	10.89
FLpaddy	938.13	2.55
Built up	800.96	2.17
Water body	1679.87	4.56
Total	**36,856.43**	**100.00**

4.7 Overall Validation

Overall validation was conducted to estimate all categories across the VCD subsets. The Cohen's kappa coefficient was 0.77 with an overall accuracy of 79 % (Table 17). Similarly, [61] applied GeoEYE and using a combination of multi-scale image segmentation and rule set approach for tropical agricultural land use classification, which give the mean kappa coefficient of 0.77. While, the other classifier consisting of Mahalanobis Distance (MD), K-NN, SVM were performed to rubber tree growth map using SPOT-5 data [52], the analyses produced the accuracy of kappa coefficient more than 0.90, which higher than our study. However, application of THAICHOTE data and OBIA of our study be able to increase the accuracy of rubber tree stand age map nearly twofold of study conduct by [62], the OBIA phenological analysis of Landsat time series data for distinguishing rubber tree stand age into older 6 years old and less than 6 years old with a quite low kappa coefficient of 0.42. However, the application of Landsat data a moderate resolution satellite imagery for rubber tree stage plantations mapping could be improved by integrated PBIA and OBIA tree growth model, which produced kappa coefficient of 0.75 [54].

The accuracy of MidR (rubber trees 4-7 years) was less than other rubber categories with user and producer accuracies of 69.23% and 87.71%, respectively. Errors and difficulties encountered were inherent from mixed, diverse ground surface conditions, small agricultural parcels and the lack of consistent patterns of land use with drought and flooding sometimes occurring in the same year. Dynamic land use planning, infrastructure development and uncertain policy in the support of farmers support trends to shape the LCLU types. The appropriateness of this approach significantly differentiated SaplingR from the other stages of rubber plantations and other LCLU types. The ESP-2 tool automated working of OBIA was applied to the identification of coarse scale by which the separability of SaplingR was apparent. The application of imagery in the defoliation period to discriminate MatureR from the very dense forests has the drawback of some difficulty in data acquisition.

5. CONCLUSION

A synergistic approach that integrated OBIA, rubber tree phenology, satellite-derived indices, vegetation canopy density (VCD), feature selection, and intensive ground observation to map different stages of rubber plantations was applied to THAICHOTE data. Two levels of classification based on OBIA approach were performed for discriminating different of stand age rubber plantations from the other LCLU types in northeasternmost, Thailand. At the first level, multi-scale image segmentation of pansharpened imagery was performed to divide the image set into objects with different spectral and spatial characteristics. Incorporating the NDVI and BI into the objects, the image set was subdivided into four different subsets of VCD. Analyses were then performed on each of VCD subsets at the next level classification by using certain and a range of different approaches to discriminate stand age rubber tree plantations.

The application of rubber tree phenology with mature rubber stands older than 7 years old shedding their leaves in February provoked the difference in NDVI values, which led to the differentiation between mature rubber trees more than 7 years old and very dense forest under the high VCD regions. A highly reliable result was obtained, with RMSE = 0.92% of the reference. For distinguishing the middle-age rubber plantations between 4-7 years old within the moderate VCD regions, the FSO tool was applied for feature optimization, which consisted of 11 layer values, 5

geometry and 5 texture features as inputs for the CART classifier and resulted in a high Cohen's kappa coefficient. Regarding the young rubber plantations between 1-4 years old with intercropping and herbaceous plants under the low VCD regions, the feature optimization comprised 11 layer values, 4 geometries, and 7 textures and yielded satisfactory results with a high Cohen's kappa coefficient. For discriminating the newly planted sapling rubber trees less than 1 years old dominated by bare fallow land within the very low VCD regions, the texture feature of GLCM Entropy (all dir.) PAN was applied, which resulted in very large entropy in contrast to that of the fallow bare land and paddy fields with dry stubble cover. The RMSE was 1.76% of the reference. The final results included the mapping of different stages of rubber plantations and their associated areas with an overall accuracy of 79 % and Cohen's kappa coefficient of 0.77.

Any particular method cannot be adapted to the application of high-resolution satellite data for different stages of rubber plantations precision mapping. The integration of satellite-derived indices, image texture, plant phenology, intensive field observations based on OBIA approach plays a key role in a precision mapping for supporting land use and land cover change analysis via using GIS and remote sensing technology.

This study is a limitation of THAICHOTE data, in which there are no shortwave infrared and thermal bands. For future work, the shortwave infrared and thermal bands from the other satellite such as Landsat or Sentinel-2 could be used to enhance the accuracy of rubber plantations and may be useful to determine the vegetation water content and burnt areas. The temporal data of vegetation indices could be taken to capture the phenological events of each different stages of rubber tree plantation to improve map accuracy. Moreover, as rubber trees require uplands and well-drained soil, using additional landforms can exclude areas of no-rubber-tree plantations. Those areas are the low lands with poorly drained soil that are unsuitable for rubber trees.

6. ACKNOWLEDGEMENTS

REFRENCES

[1] K.P. Prabhakaran Nair, "*8 - Rubber (Hevea brasiliensis) The Agronomy and Economy of Important Tree Crops of the Developing World*", London: Elsevier, 2010, pp.237-273.

[2] International Rubber Study Group, "*Statistical summary of world rubber situation*", [Online]. Available: http://www.rubberstudy.com/ documents/WebSiteData_Aug2017.pdf. [Accessed 4 December 2017].

[3] Office of Agricultural Economics Thailand, "*Base data of Agricultural Economics 2016. Agriculture Statistics No. 402*", Bangkok, Thailand: Office of Agricultural Economics, 2016.

[4] C. Mongkolsawat and W. Putklang, "Rubber tree expansion in forest reserve and paddy field across the Greater Mekong Sub-Region, northeast Thailand based on remotely sensed imagery", *33rd Asian Conference on Remote Sensing*, 2012.

[5] W. Koedsin and A. Huete, "Mapping rubber tree stand age using pléiades satellite imagery: A case study in Thalang District, Phuket, Thailand", *Engineering Journal*, Vol.19, No.4, 2015, pp.45-56.

[6] I. P. A. Shidiq and M.H. Ismail, "Stand age model for mapping spatial distribution of rubber tree using remotely sensed data in Kedah, Malaysia", *Jurnal Teknologi*, Vol.78, No.5, 2016, pp.239-244.

[7] Z. Li and J.M. Fox, "Rubber Tree Distribution Mapping in Northeast Thailand", *International Journal of Geosciences*, Vol.2, 2011, pp.573-584.

[8] Z. Li and J.M. Fox, "Mapping rubber tree growth in mainland Southeast Asia using time-series MODIS 250 m NDVI and statistical data", *Applied Geography*, Vol.32, No.2, 2012, pp.420-432.

[9] B.C.B. Hernandez and A.C. Blanco, "Rapid assessment of rubber tree plantation areas in mindanao Island, Philippines using landsat technology", *34th Asian Conference on Remote Sensing*, 2013.

[10] Y. Li and G. Liu, "Vegetation change detection based on TM and SPOT images spectrum fusion in the typical area of Xishuangbanna area", *Advanced Materials Research*, Vol.347, No.353, 2012, pp.2393-2399.

[11] Z.C. Sun, P. Leinenkugel, H.D. Guo, C. Huang, and C. Kuenzer, "Extracting distribution and expansion of rubber plantations from

Landsat imagery using the C5.0 decision tree method", *Journal of Applied Remote Sensing*, Vol.11, No.2, 2017.

[12] J.W. Dong, X.M. Xiao, B.Q. Chen, N. Torbick, C. Jin, G.L. Zhang, and C. Biradar, "Mapping deciduous rubber plantations through integration of PALSAR and multi-temporal Landsat imagery", *Remote Sensing of Environment*, Vol. 134, 2013, pp.392-402.

[13] J. Miettinen, W.J. Tan, S.C. Liew, and L.K. Kwoh, "Identification of woody plantation species in insular southeast Asia using 50 m resolution ALOS PALSAR mosaic", *31st Asian Conference on Remote Sensing*, 2010.

[14] B.H. Trisasongko, "Mapping stand age of rubber plantation using ALOS-2 polarimetric SAR data", *European Journal of Remote Sensing*, Vol. 50, No.1. 2017, pp.64-76.

[15] B.H. Trisasongko, D.J. Paull, and D.R. Panuju, "Interferometric processing of C-band SAR data for the improvement of stand age estimation in rubber plantation", *Proceedings of SPIE - The International Society for Optical Engineering*, 2015.

[16] Geo-Informatics and Space Technology Development Agency, "*The project of supporting geoinformatics and satellite imagery to verify the farmer's land ownership with tapped rubber plantation area exceeds 15 rai. Thailand*", 2015.

[17] T. Blaschke, "Object based image analysis for remote sensing", *ISPRS Journal of Photogrammetry and Remote Sensing*, Vol. 65, No.1. 2010, pp.2-16.

[18] Z. Xie, C. Roberts, and B. Johnson, "Object-based target search using remotely sensed data: A case study in detecting invasive exotic Australian Pine in south Florida", *ISPRS Journal of Photogrammetry and Remote Sensing*, Vol. 63, No.6. 2008, pp.647-660.

[19] Gibbes, C., Adhikari, S., Rostant, L., Southworth, J., & Qiu, Y. L. "Application of Object Based Classification and High Resolution Satellite Imagery for Savanna Ecosystem Analysis", *Remote Sensing*, Vol.2, No.12, 2010, pp.2748-2772.

[20] J.S. Rawat and M. Kumar, "Monitoring land use/cover change using remote sensing and GIS techniques: A case study of Hawalbagh block, district Almora, Uttarakhand, India", *Egyptian Journal of Remote Sensing and Space Science*, Vol.18, No.1, 2015, pp.77-84.

[21] T, Blaschke, G.J. Hay, M. Kelly, S. Lang, P. Hofmann, E. Addink, and D. Tiede, "Geographic Object-Based Image Analysis - Towards a new paradigm", *ISPRS Journal of Photogrammetry and Remote Sensing*, Vol.87, 2014, pp.180-191.

[22] S.W. Myint, P. Gober, A. Brazel, S. Grossman-Clarke, and Q.W. Weng, "Per-pixel vs. object-based classification of urban land cover extraction using high spatial resolution imagery", *Remote Sensing of Environment*, Vol.115, No.5, 2011, pp.1145-1161.

[23] R. C. Estoque, T. Murayama, and C.M. Akiyama, "Pixel-based and object-based classifications using high- and medium-spatial-resolution imageries in the urban and suburban landscapes", *Geocarto International*, Vol.30, No.10, 2015, pp.1113-1129.

[24] S. Agarwal, L.S. Vailshery, M. Jaganmohan, and H. Nagendra, "Mapping Urban Tree Species Using Very High Resolution Satellite Imagery: Comparing Pixel-Based and Object-Based Approaches", *ISPRS Journal of Photogrammetry and Remote Sensing*, Vol.2, No.1, 2013, pp.220-236.

[25] T.G. Whiteside, G.S. Boggs, and S.W. Maier, "Comparing object-based and pixel-based classifications for mapping savannas", *International Journal of Applied Earth Observation and Geoinformation*, Vol.13, No.6, 2011, pp.884-893.

[26] M.S. Tehrany, B. Pradhan, and M.N. Jebuv, "A comparative assessment between object and pixel-based classification approaches for land-use/land-cover mapping using SPOT 5 imagery", *Geocarto International*, Vol.29, No.4, 2014, pp.351-369.

[27] L. Xun, and L. Wang, "An object-based SVM method incorporating optimal segmentation scale estimation using Bhattacharyya Distance for mapping salt cedar (Tamarisk spp.) with QuickBird imagery", *Giscience & Remote Sensing*, Vol.52, No.3, 2015, pp.257-273.

[28] Royal Thai Survey Department, "*Thailand L7017S Series 1: 50,000 Scale Topographic Maps*", 1994.

[29] Thai Meteorological Department, "*Climatological data of Thailand for 30-year (1981-2010)*", Bangkok Thailand, 2015.

[30] Soil Survey Staff, "*Keys to Soil Taxonomy*", 12th Edition, USDA-Natural Resources Conservation Service, Washington, DC, 2014.

[31] Land Development Department, "*Soil Series Map, scale 1:50000*", Bangkok, Thailand, 2000.

[32] Office of Agricultural Economics Thailand, "*Base data of Agricultural Economics 2010*", Agriculture Statistics No.416, Office of Agricultural Economics, Bangkok, Thailand, 2010.

[33] L. Meng and Y. Liang, "Modeling the volatility of futures return in rubber and oil-A Copula-based GARCH model approach", *Economic Modelling*, Vol. 35, 2013, pp.576-581.

[34] Trimble, "*eCognition Developer 8.9 User Guide*", Munich, Germany: Trimble Germany GmbH, 2013.

[35] Land Development Department, "*Impact assessment of planting rubber-trees on sandy soils in ne Thailand*", TICA report –March 2010, [Online]. Available: http://www.ldd.go.th/www/files/74814.pdf

[36] T.W. Giambelluca, R.G. Mudd, W. Liu, A.D. Ziegler, N. Kobayashi, T.O. Kumagai, and P. Kasemsap, "Evapotranspiration of rubber (Hevea brasiliensis) cultivated at two plantation sites in Southeast Asia", *Water Resources Research*, Vol. 52, No.2, 2016, pp.660-679.

[37] N. Phongaksorn, N.K. Tripathi, S. Kumar, and P. Soni, "Inter-Sensor Comparison between THEOS and Landsat 5 TM Data in a Study of Two Crops Related to Biofuel in Thailand", *Remote Sensing*, Vol.4, No.2, 2012, pp.354-376.

[38] Y. Zhang, "A new automatic approach for effectively fusing Landsat 7 as well as IKONOS images", *International Geoscience and Remote Sensing Symposium (IGARSS)*, 2002, pp.626-632.

[39] L. Dragut, O. Csillik, C. Eisank, and D. Tiede, "Automated parameterisation for multi-scale image segmentation on multiple layers", *Isprs Journal of Photogrammetry and Remote Sensing*, Vol. 88, 2014, pp.119-127.

[40] R.L. Lawrence and W.J. Ripple, "Comparisons among vegetation indices and bandwise regression in a highly disturbed, heterogeneous landscape: Mount St. Helens, Washington", *Remote Sensing of Environment*, Vol. 64, No.1, 1998, pp.91-102.

[41] R. Mathieu, M. Pouget, B. Cervelle, and R. Escadafal, "Relationships between satellite-based radiometric indices simulated using laboratory reflectance data and typic soil color of an arid environment", *Remote Sensing of Environment*, Vol. 66, No.1, 1998, pp.17-28.

[42] G.F. Jenks, "*The data model concept in statistical mapping*", In K. Frenzel (Ed.), International Yearbook of Cartography, USA.

ICA: Rand McNally & Co, Vol.7, 1967, pp.186-190.

[43] A.S. Laliberte, D.M. Browning, and A. Rango, "A comparison of three feature selection methods for object-based classification of sub-decimeter resolution UltraCam-L imagery", *International Journal of Applied Earth Observation and Geoinformation*, Vol.15, 2012, pp.70-78.

[44] R.G. Congalton, "A review of assessing the accuracy of classifications of remotely sensed data", *Remote Sensing of Environment*, Vol.37, No.1, 1991, pp. 35-46.

[45] A.J. Viera and J.M. Garrett, "Understanding interobserver agreement: the kappa statistic", *Family Medicine*, Vol.37, No.5, 2005, pp.360-363.

[46] M. Gianinetto, M. Rusmini, G. Candiani, G. Dalla Via, F. Frassy, and P. Maianti, "Hierarchical classification of complex landscape with VHR pan-sharpened satellite data and OBIA techniques", *European Journal of Remote Sensing*, Vol.47, 2014, pp. 229-250.

[47] A. B. Johnson, M. Bragais, I. Endo, B. D. Magcale-Macandog, and B. P. Macandog, "Image Segmentation Parameter Optimization Considering Within- and Between-Segment Heterogeneity at Multiple Scale Levels: Test Case for Mapping Residential Areas Using Landsat Imagery", *ISPRS International Journal of Geo-Information*, Vol.4, No.4, 2015.

[48] X. ZhangHugo, X. Feng, and P. Xiao, "Multi-scale Segmentation of High-Spatial Resolution Remote Sensing Images Using Adaptively Increased Scale Parameter", *Photogrammetric Engineering & Remote Sensing*, Vol.81, No.6, 2015, pp. 461-470.

[49] T. Kavzoglu, M. Yildiz Erdemir, and H. Tonbul, "A region-based multi-scale approach for object-based image analysis", *International Archives of the Photogrammetry, Remote Sensing and Spatial Information Sciences - ISPRS Archives*, 2016.

[50] F. Hájek, "Object-oriented classification of remote sensing data for the identification of tree species composition", *Proceedings of ForestSat 2005 conference*, 2005. pp.16-20.

[51] G. Mallinis, N. Koutsias, M. Tsakiri-Strati, and M. Karteris, "Object-based classification using Quickbird imagery for delineating forest vegetation polygons in a Mediterranean test site", *ISPRS Journal of Photogrammetry and Remote Sensing*, Vol.63, No.2, 2008, pp.237-250.

[52] H. Dibs, M. O. Idrees, and G. B. A. Alsalhin, "Hierarchical classification approach for mapping rubber tree growth using per-pixel and object-oriented classifiers with SPOT-5 imagery", *The Egyptian Journal of Remote Sensing and Space Science*, Vol.20, No.1, 2017, pp.21-30.

[53] D. Zhai, J. Dong, G. Cadisch, M, Wang, W. Kou, J, Xu, "Comparison of Pixel- and Object-Based Approaches in Phenology-Based Rubber Plantation Mapping in Fragmented Landscapes", *Remote Sensing*, Vol.10, No.1. 2018.

[54] G. Chen, J.-C, Thill, S. Anantsuksomsri, N. Tontisirin, and R. Tao, "Stand age estimation of rubber (Hevea brasiliensis) plantations using an integrated pixel- and object-based tree growth model and annual Landsat time series", *ISPRS Journal of Photogrammetry and Remote Sensing*, Vol.144, 2018. pp.94-104.

[55] M. Kim, T. A, Warner, M. Madden, and D. S. Atkinson, "Multi-scale GEOBIA with very high spatial resolution digital aerial imagery: scale, texture and image objects", *International Journal of Remote Sensing*, Vol.32, No.10, 2011, pp.2825-2850.

[56] A.S. Laliberte, E.L. Fredrickson, and A. Rango, "Combining decision trees with hierarchical object-oriented image analysis for mapping arid rangelands", *Photogrammetric Engineering and Remote Sensing*, Vol.73, No.2, 2007, pp.197-207.

[57] I. P. A. Shidiq, and M. H. Ismail, "Stand age model for mapping spatial distribution of rubber tree using remotely sensed data in Kedah, Malaysia", *Jurnal Teknologi*, Vol.78, No.5, 2016. pp.239-244.

[58] K. Sakayarote, and R. P. Shrestha, "Policy-driven rubber plantation and its driving factors: a case of smallholders in northeast Thailand", *International Journal of Sustainable Development and World Ecology*, Vol.24, No.1, 2017, pp.15-26.

[59] M. Marimin, A. Wibisono, and A. D. Muhammad, "Decision Support System for Natural Rubber Supply Chain Management Performance Measurement: A Sustainable Balanced Scorecard Approach", *Journal of Supply Chain Management*, Vol.6, No.2, 2017, pp.60-74.

[60] D. Hougni, B. Chambon, E. Penot, and A. Promkhambut, "The household economics of rubber intercropping during the immature period in Northeast Thailand", *Journal of Sustainable Forestry*, Vol.37, No.8, 2018, pp. 787-803.

[61] N. Nagabhatla, and P. Kuhle, "Tropical Agrarian Landscape Classification using high-resolution GeoEYE data and segmentationbased approach", European *Journal of Remote Sensing*, Vol.49, 2016, pp. 623-642.

[62] J. A. b. A. Razak, A. R. b. M. Shariff, N. b. Ahmad, and M. Ibrahim Sameen, "Mapping rubber trees based on phenological analysis of Landsat time series data-sets", *Geocarto International*, Vol.33, No.6, 2018, pp. 627-650.
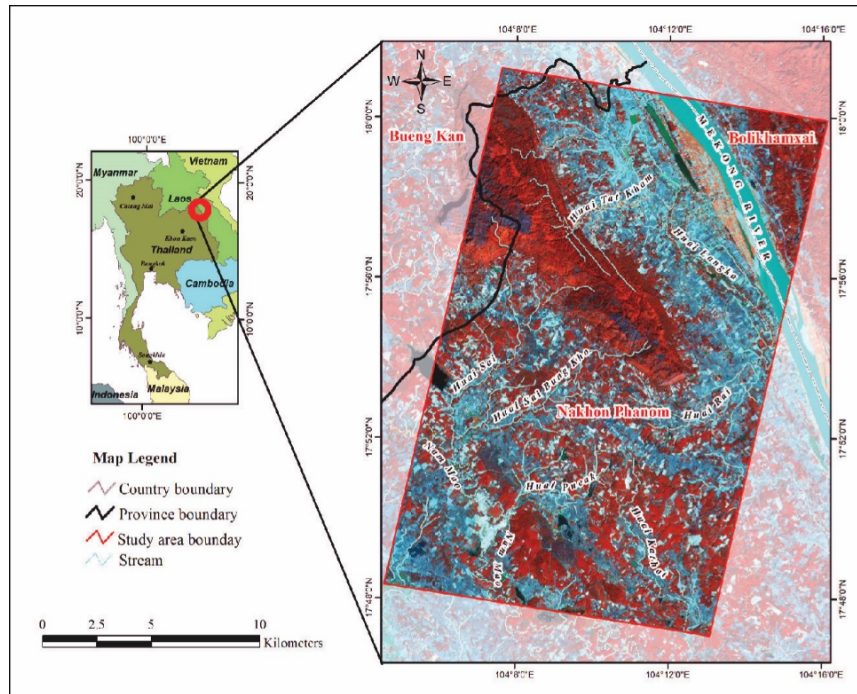
Figure 1: The site of study area. Image Background: THAICHOTE image acquired 15th December 2012, Band Combination 4 2 3.
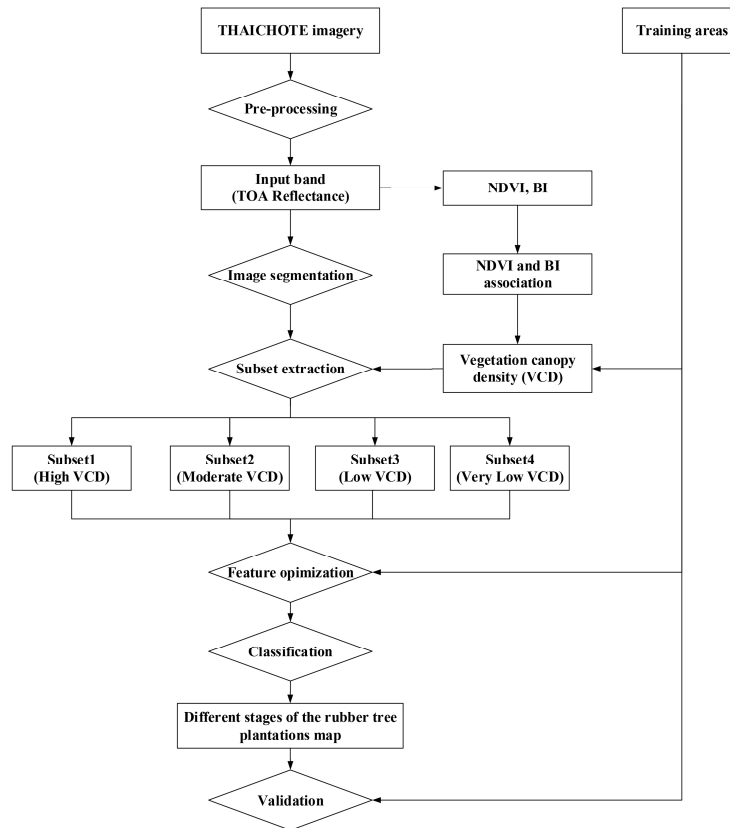

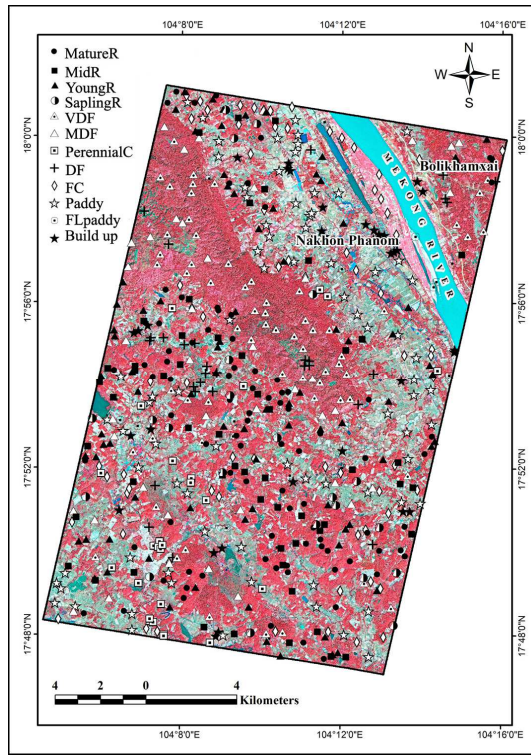*Figure 2: The flowchart of the study*

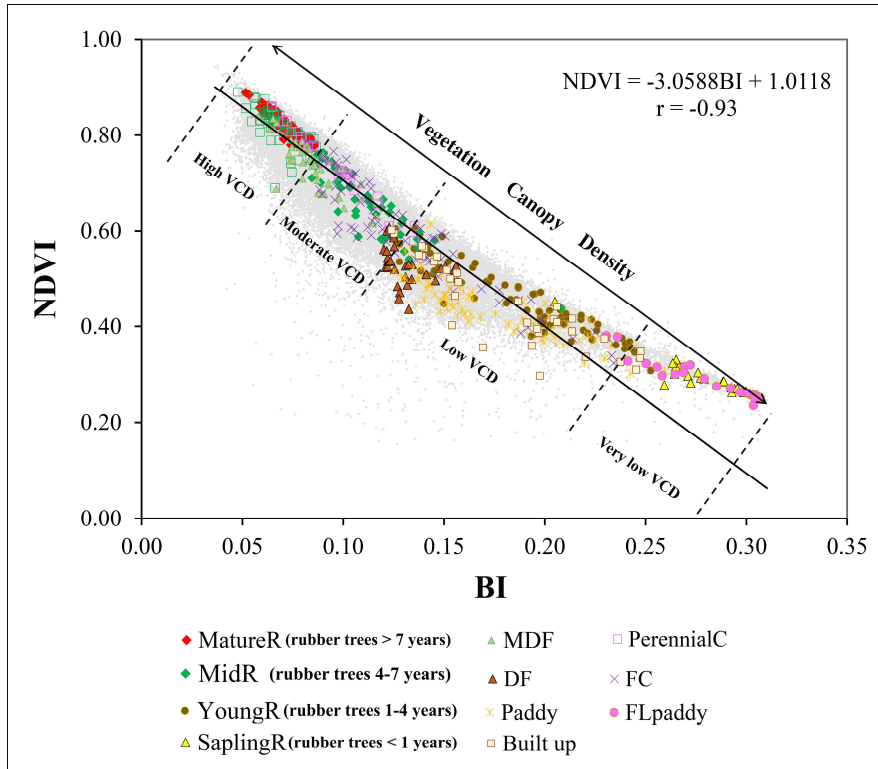*Figure 4: Locations of training areas for subdivision into four VCD subsets.*

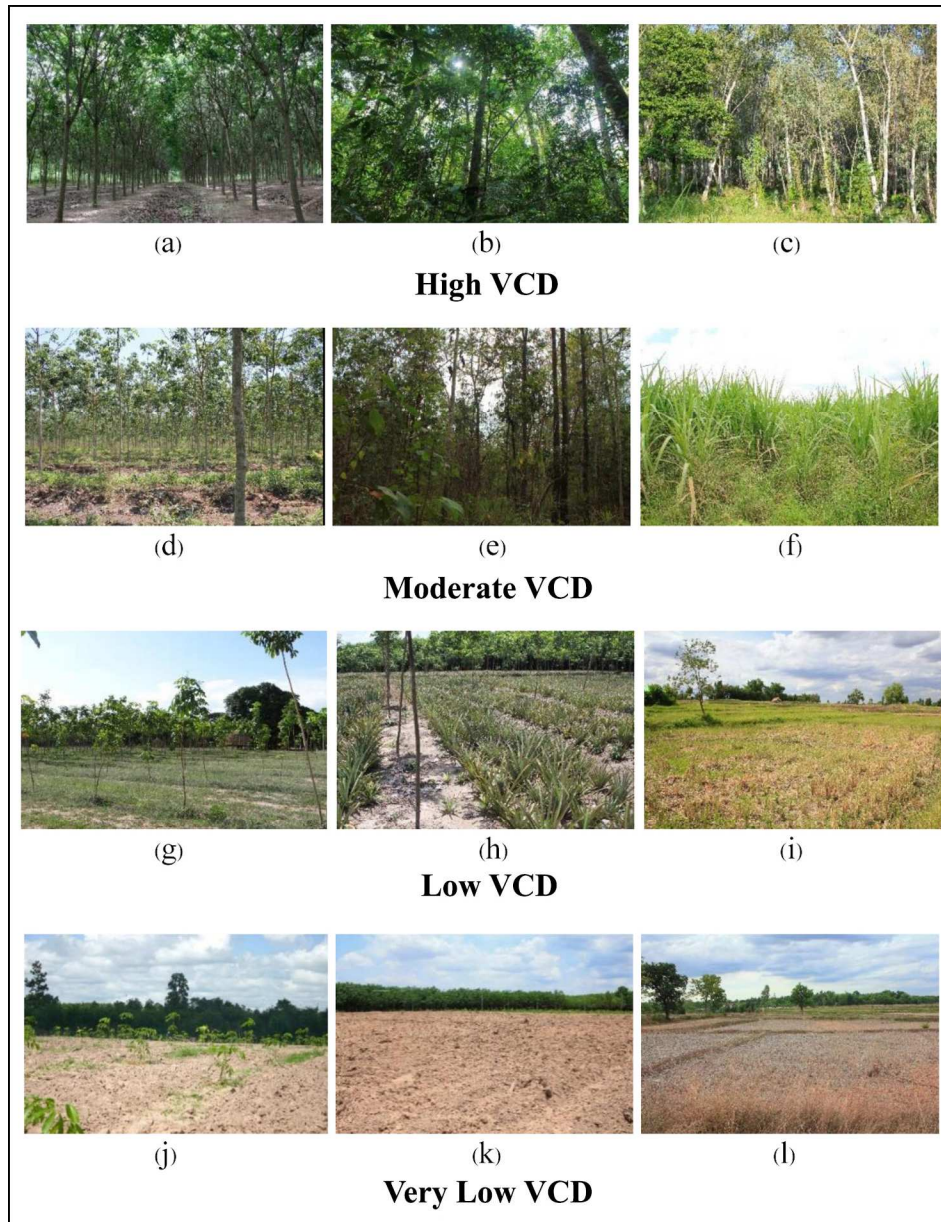*Figure 5: The four VCD subset regions resulting from associating NDVI and BI.*

Figure 6: Ground observations, High VCD: (a) Rubber trees > 7 years (MatureR), (b) Very dense forest (VDF), (c) forest plantation; Moderate VCD: (d) Rubber trees 4-7 years (MidR), (e) Moderately dense forest (MDF), (f) Field crop and herbaceous plants (FC); Low VCD: (g) Rubber trees 1-4 years with herbaceous plants (YoungR), (h) Rubber trees 1-4 years with intercropping (YoungR), (i) Paddy field with small grass and herbaceous(Paddy); Very Low VCD: (j) Rubber trees < 1 years old (SaplingR), (k) Fallow bare land and paddy field (FLpaddy) and (l) Paddy field with dry rice stubble cover.
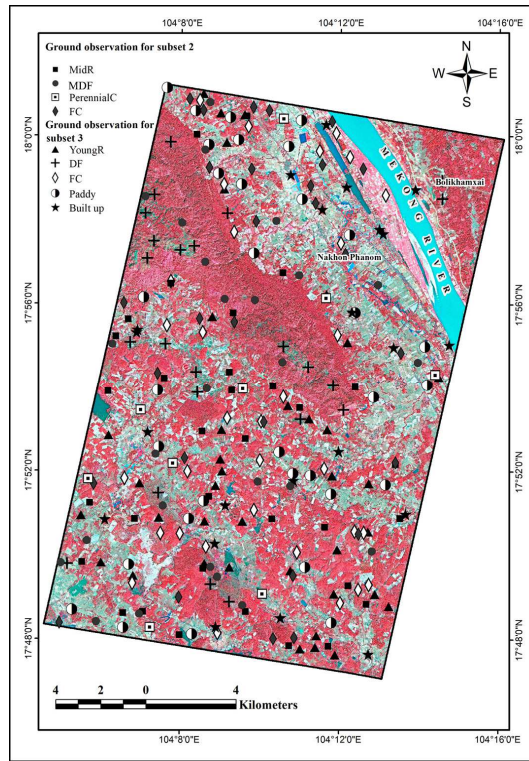
Figure 7: Locations of ground observations used to validate classification within Moderate VCD and Low VCD regions.
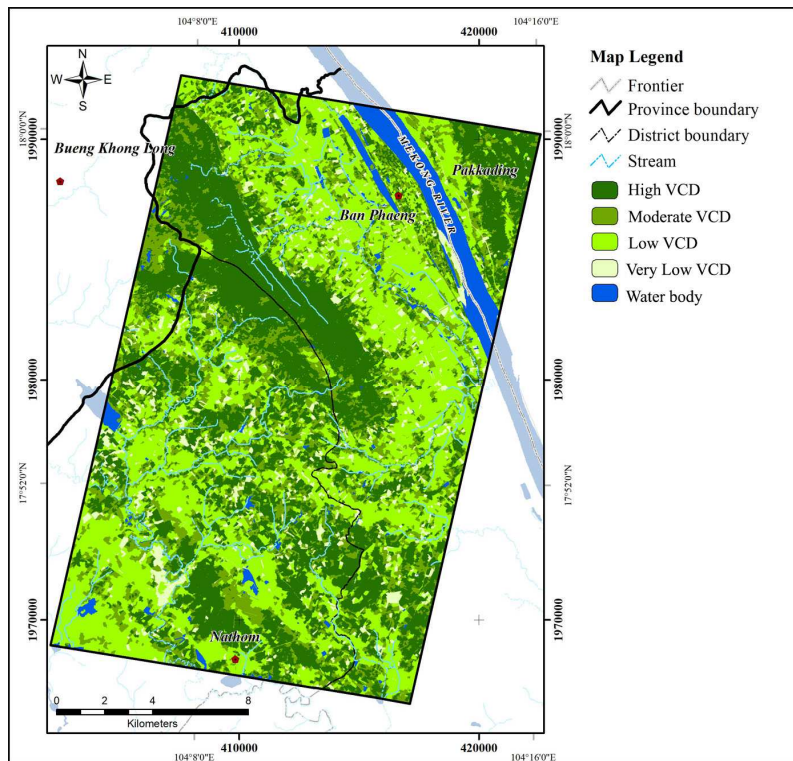

Figure 8. The four VCD subsets that consist of MatureR, MidR, YoungR and SaplingR, each found confused with other LCLU types.
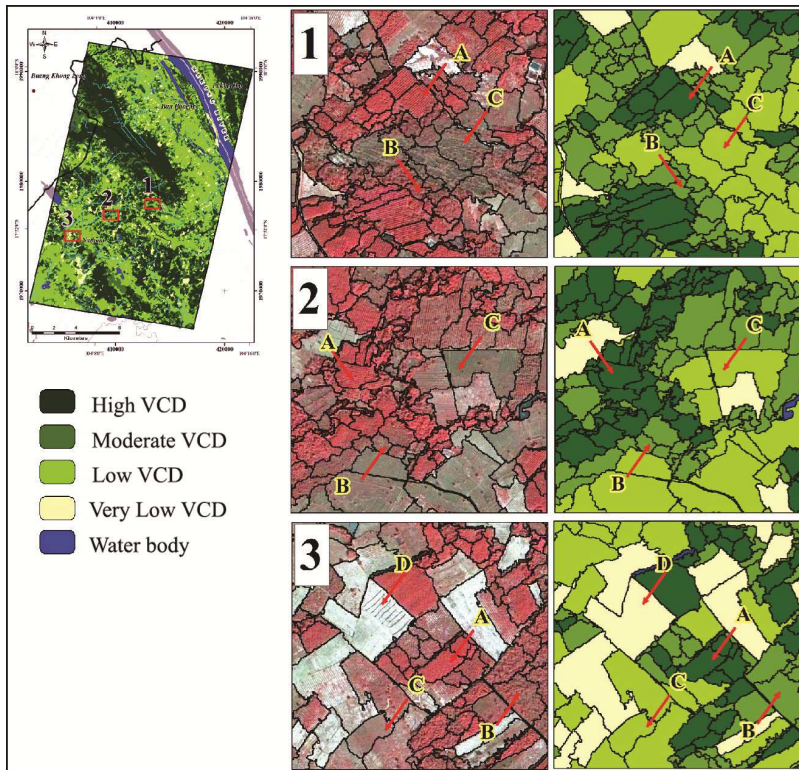
*Figure 9: Multi-scale segmentation OBIA and the association of NDVI with BI
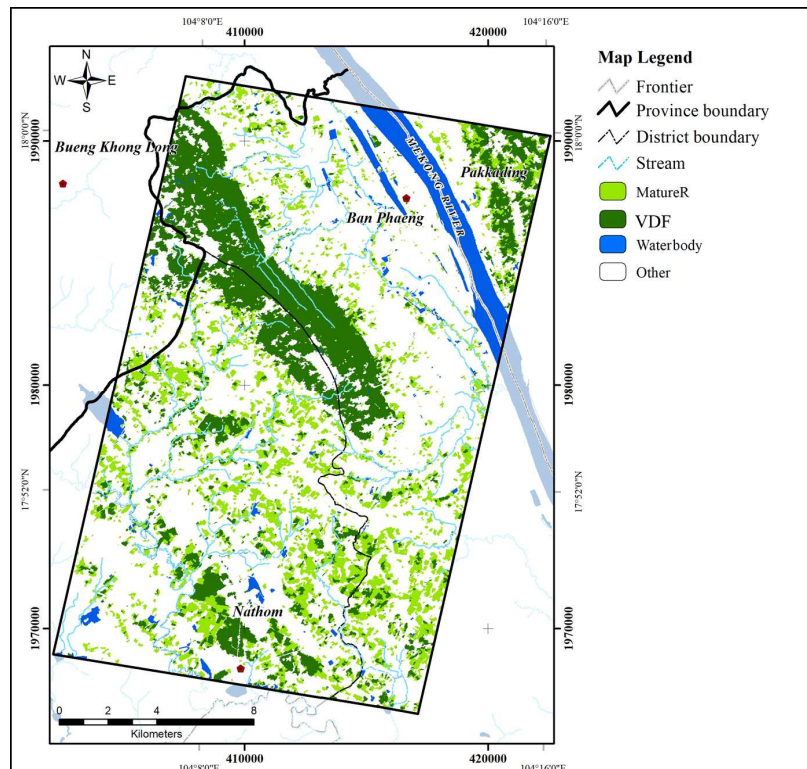(A = High VCD, B = Moderate VCD, C = Low VCD, and D = Very Low VCD).*

Figure 12: The distribution of MatureR (rubber trees > 7 years) and very dense forest areas within High VCD regions.
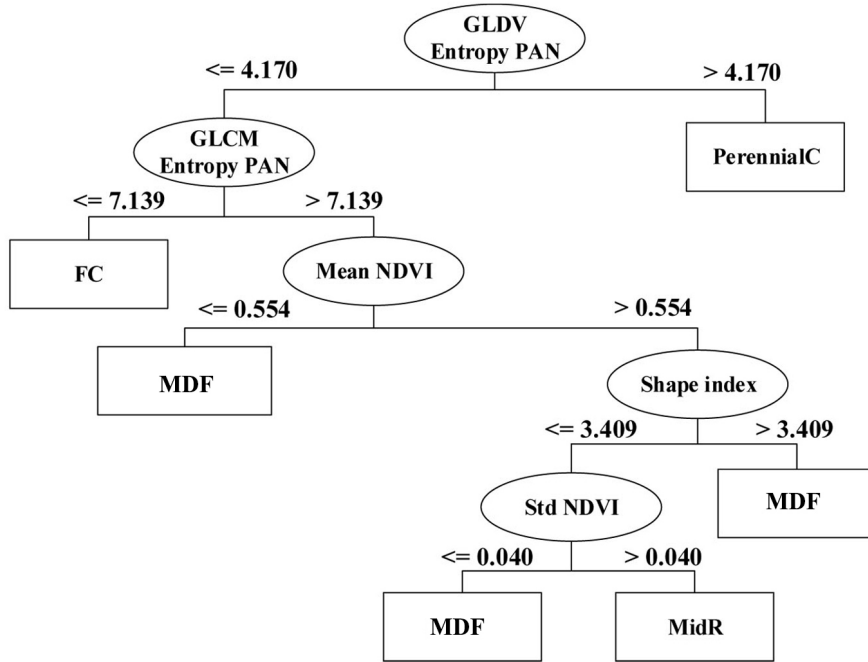
Figure 14: CART model to estimate the MidR (rubber trees 4-7 years) and other LCLU within moderate VCD regions.
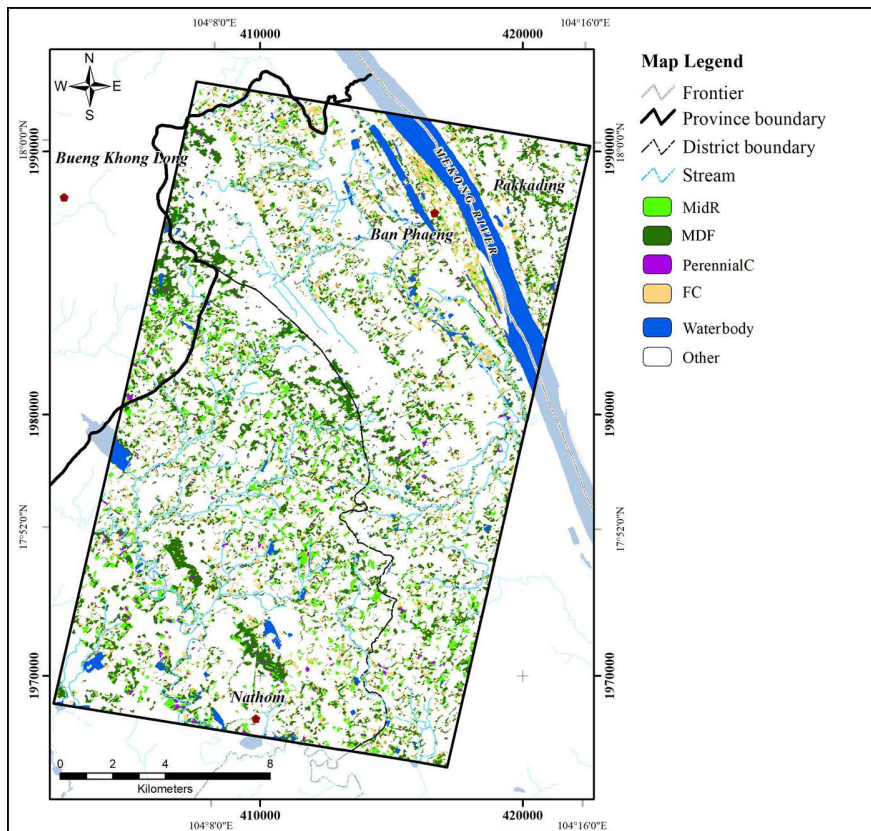

Figure 15: The distribution of MidR (rubber trees 4-7 years) and other LCLU within moderate VCD regions.

Figure 17: CART model to estimate the YoungR (rubber trees 1-4 years) and other LCLU within low VCD regions.

Figure 18: The distribution of YoungR (rubber trees 1-4 years) and other LCLU within low VCD regions.

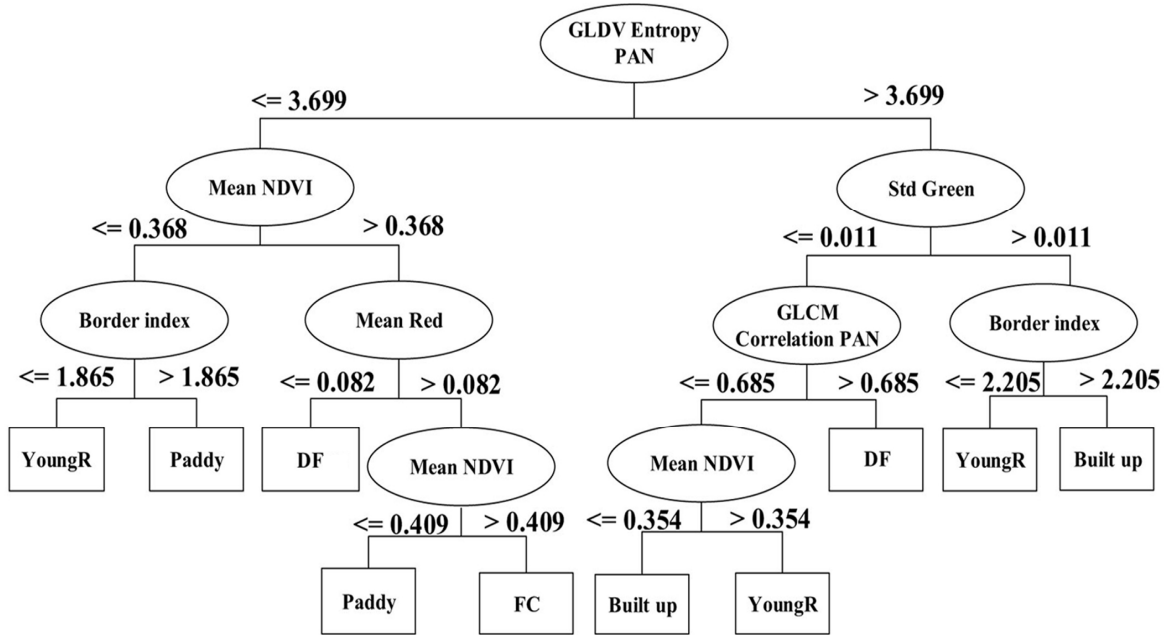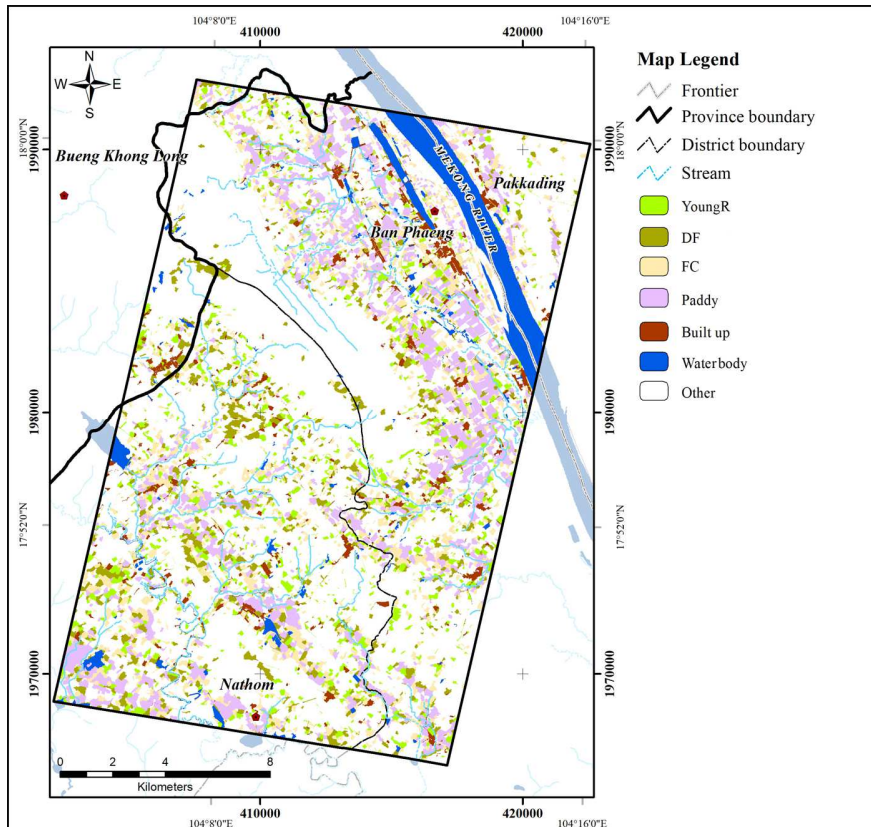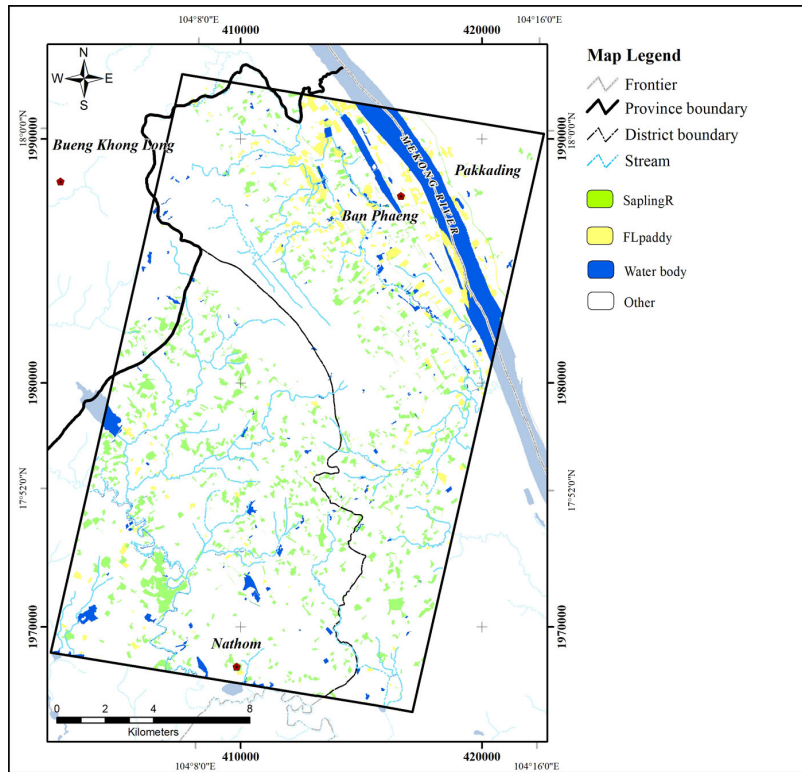*Figure 21: The distribution of SaplingR (rubber trees < 1 years old) and FLpaddy within within very low VCD.*
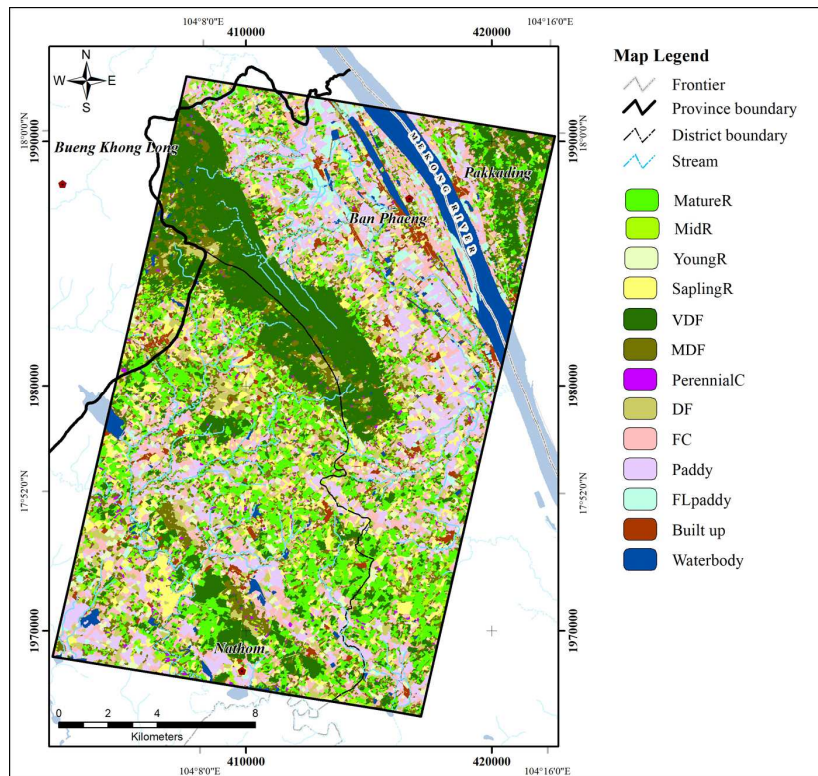

Figure 23: The distribution of mature, middle, young and sapling-aged rubber tree plantations and other LCLU types in the study area.

Table 2: Number of training areas.

Cover type	Number of training areas
Mature rubber trees older than 7 years old (MatureR)	89
Middle-age rubber trees between 4 to 7 years old (MidR)	55
Young rubber trees between 1 to 4 years old dominated by intercropping and herbaceous plants (YoungR)	84
Newly planted sapling rubber trees less than 1 years old dominated by bare fallow land (SaplingR)	22
Very Dense Forest (VDF)	63
Moderately Dense Forest (MDF)	42
Perennial crops and orchard (PerennialC)	29
Degraded forest in association with grass and outcrop (DF)	30
Field crop and herbaceous plants (FC)	70
Paddy fields with small grass and herbaceous and some few sparse native tree (Paddy)	79
Fallow bare land and paddy field with dry stubble cover (FLpaddy)	21
Urban and Built up areas (Built up)	36
Total	620

Table 8: Features selected for CART classification for distinguishing MidR within moderate VCD region.

Category	Object Feature	Definition
Layer values	1. Mean Blue	Mean values of image object in the Blue band.
	2. Mean Red	Mean values of image object in the Red band.
	3. Mean NIR	Mean values of image object in the NIR band.
	4. Mean NDVI	Mean values of image object in the NDVI.
	5. Mean BI	Mean values of image object in the BI.
	6. Std. Blue	Standard deviation image object in the Blue band.
	7. Std. Green	Standard deviation image object in the Green band.
	8. Std. Red	Standard deviation image object in the Red band.
	9. Std. NIR	Standard deviation image object in the NIR band.
	10. Std. BI	Standard deviation image object in the BI.
	11. Std. NDVI	Standard deviation image object in the NDVI.
Geometry	12. Asymmetry	The ratio of the lengths of minor and the major axes.
	13. Shape index	The border length feature of the image object divided by four times the square root of its area.
	14. Elliptic fit	An ellipse with the same area as the selected image object.
	15. Rectangular Fit	A rectangule with the same size as the considered image object.
	16. Roundness	The difference of the enclosing ellipse and the enclosed ellipse.
Texture	17. GLCM Correlation PAN	Grey level co-occurrence matrix correlation for PAN.
	18. GLCM Entropy PAN	Grey level co-occurrence matrix entropy for PAN.
	19. GLCM Dissimilarity PAN	Grey level co-occurrence matrix dissimilarity for PAN.
	20. GLDV Entropy PAN	Grey level difference vector entropy for PAN.
	21. GLDV Mean PAN	Grey level difference vector mean for PAN.

Table 11: Features selected for CART Classification for distinguishing YoungR within low VCD region.

Category	Object Feature	Definition
Layer values	1. Mean Green	Mean values of image object in the Green band.
	2. Mean Red	Mean values of image object in the Red band.
	3. Mean NIR	Mean values of image object in the NIR band.
	4. Mean NDVI	Mean values of image object in the NDVI.
	5. Mean BI	Mean values of image object in the BI.
	6. Std. Blue	Standard deviation image object in the Blue band.
	7. Std. Green	Standard deviation image object in the Green band.
	8. Std. Red	Standard deviation image object in the Red band.
	9. Std. NIR	Standard deviation image object in the NIR band.
	10. Std. BI	Standard deviation image object in the BI.
	11. Std. NDVI	Standard deviation image object in the NDVI.
Geometry	12. Asymmetry	The ratio of the lengths of minor and major axes.
	13. Border index	The ratio between the border lengths of the image object and the smallest enclosing rectangle.
	14. Rectangular Fit	A rectangule with the same size as the considered image object.
	15. Roundness	The difference of the enclosing ellipse and the enclosed ellipse.
Texture	16. GLCM Correlation PAN	Grey level co-occurrence matrix correlation for PAN.
	17. GLCM Entropy PAN	Grey level co-occurrence matrix entropy for PAN.
	18. GLCM Dissimilarity PAN	Grey level co-occurrence matrix dissimilarity for PAN.
	19. GLCM Contrast PAN	Grey level co-occurrence matrix contrast for PAN.
	20. GLDV Entropy PAN	Grey level difference vector entropy for PAN.
	21. GLDV Mean PAN	Grey level difference vector mean for PAN.
	22. GLDV Contrast PAN	Grey level difference vector contrast for PAN.

Table 17: Agreement between field-based observations and image-based classification for all categories

Image based classification	Field based observation													Accuracy (%)	
	1	2	3	4	5	6	7	8	9	10	11	12	Total	User's	Producer's
1	24	0	0	0	0	0	0	0	0	0	7	0	31	77.42	96.00
2	0	32	0	0	0	0	0	1	2	2	0	1	38	84.21	88.89
3	0	0	27	4	2	3	2	0	1	0	0	0	39	69.23	87.71
4	0	0	0	16	2	1	0	0	2	0	0	0	21	76.19	57.14
5	0	0	0	8	15	0	0	0	0	0	0	0	23	65.22	75.00
6	0	0	3	0	1	21	1	0	1	0	0	0	27	77.78	80.77
7	0	0	1	0	0	0	6	0	0	0	0	0	7	85.71	66.67
8	0	0	0	0	0	0	0	13	0	2	0	0	15	86.67	72.22
9	0	1	0	0	0	1	0	2	37	2	1	1	45	82.22	84.09
10	0	1	0	0	0	0	0	1	1	25	1	0	29	86.21	80.65
11	1	0	0	0	0	0	0	0	0	0	4	0	5	80.00	30.77
12	0	2	0	0	0	0	0	1	0	0	0	17	20	85.00	89.47
Total	25	36	31	28	20	26	9	18	44	31	13	19	300		
Overall accuracy (%)	**79.00**														
Cohen's kappa coefficient	**0.77**														

LCLU type: 1= SaplingR; 2= YoungR; 3= MidR; 4= MatureR; 5= VDF; 6= MDF; 7= PerennialC; 8= DF; 9= FC; 10= Paddy; 11= FLpaddy; 12= Built up